Published in final edited form as:

Arterioscler Thromb Vasc Biol. 2021 December ; 41(12): 2943–2960. doi:10.1161/ATVBAHA.121.316707.

CCM3 loss-induced lymphatic defect is mediated by the augmented VEGFR3-ERK1/2 signaling

Lingfeng Qin[1,*], **Haifeng Zhang**[1,*], **Busu Li**[1], **Quan Jiang**[1], **Francesc Lopez**[2], **Wang Min**[1], **Jenny Huanjiao Zhou**[1]

[1]Interdepartmental Program in Vascular Biology and Therapeutics, Department of Pathology, Yale University School of Medicine, New Haven, CT.

[2]Yale Center for Genome Analysis, Cancer Department of Genetics, Yale University School of Medicine, New Haven, CT.

Abstract

Objective: Cerebral cavernous malformations (CCMs) can happen anywhere in the body, although they most commonly produce symptoms in the brain. The role of CCM genes in other vascular beds outside the brain and retina are not well-examined, although the 3 CCM-associated genes (*CCM1*, *CCM2* and *CCM3*) are ubiquitously expressed in all tissues. We aimed to determine the role of *CCM* gene in lymphatics.

Approach and Results: Mice with an inducible pan-endothelial cell (EC) or lymphatic EC deletion of *Ccm3* (*Pdcd10*^{ECKO} or *Pdcd10*^{LECKO}) exhibit dilated lymphatic capillaries and collecting vessels with abnormal valve structure. Morphological alterations were correlated with lymphatic dysfunction in *Pdcd10*^{LECKO} mice as determined by Evans blue dye and FITC-dextran transport assays. *Pdcd10*^{LECKO} lymphatics had increased vascular endothelial growth factor receptor-3 (VEGFR3)-ERK1/2 signaling with lymphatic hyperplasia. Mechanistic studies suggested that VEGFR3 is primarily regulated at a transcriptional level in Ccm3-deficient LECs, in a NF-κB-dependent manner. CCM3 binds to importin alpha 2/karyopherin subunit alpha 2 (KPNA2), and a CCM3 deletion releases KPNA2 to activate NF-κB P65 by facilitating its nuclear translocation and P65-dependent VEGFR3 transcription. Moreover, increased VEGFR3 in LEC preferentially activates ERK1/2 signaling, which is critical for LEC proliferation. Importantly, inhibition of VEGFR3 or ERK1/2 rescued the lymphatic defects in structure and function.

Conclusion: Our data demonstrate that CCM3 deletion augments the VEGFR3-ERK1/2 signaling in lymphatic EC that drives lymphatic hyperplasia and malformation, and warrant further investigation on the potential clinical relevance of lymphatic dysfunction in CCM patients.

Please address correspondence to: Dr. Huanjiao Zhou or Dr. Wang Min, Interdepartmental Program in Vascular Biology and Therapeutics, Department of Pathology, Yale University School of Medicine, 10 Amistad St., 411B, New Haven, CT 06520, Tel: 203-785-7290; Fax: 203-737-2293; huanjiao.zhou@yale.edu or mike.wang388@gmail.com.

*These authors contributed equally.

AUTHOR CONTRIBUTIONS

HJZ and WM provided conceptualization of the study and designed all the experiments; HJZ executed and organized team members; LQ and BL did the in vivo study; HZ and QJ carried out the in vitro experiments; FL did the bioinformatics analyses; HJZ and WM analyzed the data, wrote the manuscript and provided funding sources.

c)Disclosure: None.

Keywords

Cerebral cavernous malformation (CCM); lymphatic dysfunction; CCM3; KPNA2; VEGFR3

INTRODUCTION

Cerebral cavernous malformations (CCMs) are vascular malformations comprising closely clustered, enlarged capillary channels (caverns) with a single layer of endothelium without mature vessel wall elements or normal intervening brain parenchyma. In CCMs, capillary walls are thinner than normal, less elastic, and prone to leakage [1-3]. CCMs are primarily found within the vasculature of the central nervous system (CNS, i.e., brain and spinal cord), where they increase the risk of stroke, seizures, and focal neurological deficits [3]. Approximately one in 200 people have a cavernoma. CCMs occur sporadically, and multiple occurrences of CCM are highly suggestive of a genetic origin of the disorder [4]. The concurrence of CCM and other vascular anomalies has been described previously. Cavernous malformations can happen anywhere in the body, but they most commonly produce symptoms when in the brain and spinal cord [4]. Vascular lesions found outside the CNS are associated with multiple intracranial cavernomas (cavernous malformations), retinal cavernomas, cutaneous vascular malformations, liver cavernoma, and venous anomalies [5, 6]. However, the role of CCM genes in other vascular beds and the lymphatic system has not been well-examined.

Most cases of familial CCM and more than half of the sporadic cases with multiple CCM are associated with three genes: *CCM1* (or Krev/Rap1 Interacting Trapped 1, *KRIT1*) [7], *CCM2* (or malcavernin or osmosensing scaffold for mitogen-activated protein kinase kinase-3, *OSM*) [8] and *CCM3* (or programmed cell death 10, *PDCD10*) [9]. The primary defects underlying CCMs are *CCM* gene deficiencies in vascular ECs [10-12], but mural cells and astrocytes also contribute to CCM pathogenesis [13-15]. Current mouse models inducing global-EC deletions in any one of the three *Ccm* genes (*Ccm1*, *Ccm2,* or *Ccm3*) cause CCM lesions in mouse brains and retinas that resemble human lesions [16-21]. CCM proteins regulate common pathways, including RhoA-dependent EC stress fiber formation, TGF-β/Smad/BMP-mediated endothelial-mesenchymal transition (EndMT) signaling, and MEKK3-ERK5-KLF2/4-mediated matrix remodeling. Importantly, all of these pathways contribute to the onset and progression of CCMs [16-21]. CCM1, CCM2, and CCM3 proteins are found in the same complex within the cell [22, 23] and regulate common downstream pathways [17, 24]. However, CCM3 may also act separately from CCM1 and CCM2, as *CCM3* mutations in humans often result in a more severe form of the disease [25, 26]. Consistent with human studies, mice with CCM3 loss exhibit a more severe phenotype than mice with CCM1 or CCM2 losses [27, 28]. At the molecular level, CCM3, but not CCM1 or CCM2, specifically interacts with the germinal center kinases (GCKs) STK24 and STK25 [29]. By interacting with GCK in ECs, CCM3 suppresses the exocytosis-mediated secretion of angiopoietin-2 (Angpt2) [27]. Moreover, our recent study demonstrated that CCM3 also regulates Angpt2 receptor Tie2. Specifically, we showed that a *CCM3* deletion enhances Tie2 trafficking and signaling in ECs via a caveolae-dependent mechanism [30]. These data suggest that CCM3 may have broad biological functions in various tissues by regulating

distinct effector molecules. Reports show that CCM3 regulates vascular endothelial growth factor (VEGF)-VEGF receptor 2 (VEGFR2) signaling in a context-dependent manner [31, 32]. However, the role of CCM3 in VEGFR3 signaling and lymphangiogenesis has not been investigated.

The vasculature contains blood vessels and lymphatic vessels, which are two developmentally related but functionally distinct systems. A mature lymphatic system consists of lymphatic capillaries and collecting lymphatic vessels. Lymphatic capillaries are blind-ended vessels formed from a single layer of lymphatic ECs (LECs) with very permeable, button-like junctions that allow the uptake of tissue fluid (lymph). In contrast, mature collecting lymphatic vessels are surrounded by a basement membrane, pericytes, and smooth muscle cells [33]. Collecting lymphatic vessels also have lymphatic valves to enhance the unidirectional flow of lymph [34, 35]. During valve formation, clusters of Prox1-positive lymphatic valve-covering LECs form a ring-like structure that extends and matures into V-shaped leaflets that can prevent lymph backflow [33, 34]. Lymphatic vessels express distinct cellular markers such as VEGFR3, Prox1, podoplanin, and lymphatic vessel endothelial hyaluronan receptor-1 (LYVE1). VEGFR3 is critical for both developmental angiogenesis and lymphangiogenesis. It has been reported that VEGFR3 null mice die as early as E10.5 before the formation of the lymphatic system due to a failure in remodeling of the primary vascular plexus [36]. When deficient in the VEGFR3 ligand VEGF-C, mouse embryos do not develop primitive lymph sacs or lymphatic vessels and die after E15.5 [37]. In humans, congenital hereditary lymphedema, known as Milroy disease, has been linked with a mutation in the tyrosine kinase domain of the VEGFR3 gene [38, 39]. Similarly, the *Chy* mouse mutant, a model for congenital lymphedema that contains a heterozygous mutation to deactivate VEGFR3, has abnormal cutaneous lymphatic vessels and symptoms of lymphedema [37]. Interestingly, VEGFR3 is abundant in collecting lymphatic trunks before valve formation but decreases after valve formation. Therefore, abnormally high VEGFR3 in collecting lymphatics causes immature lymphatic valves and defective lymph drainage in mice [40-42].

The VEGFR3 protein level in LECs can be regulated at multiple levels under physiological settings. The transcription factors Prox1, NF-κB, Ets, and the transcription factor T-box 1 (Tbx1) transactivate *Vegfr3* gene expression by directly binding to the *Vegfr3* gene promoter [43-45]. Notch can also transactivate the *Vegfr3* gene [46], although some reports suggest negative regulation of VEGFR3 expression by Notch signaling [46]. We have previously shown that *miR-1236* binds to the 3' untranslated region (UTR) of the *Vegfr3* mRNA and inhibits its translation, representing a post-transcriptional mechanism for VEGFR3 expression [47]. Protein stability also regulates the VEGFR3 level. Dr. Adams' group has reported a strong increase in VEGFR3 but not VEGFR2 protein in Notch-defective (*Rbpj*-deletion and *Dll4*-deletion) angiogenic retinal vessels and lung vasculatures. However, the levels of VEGFR3 mRNA were not substantially increased, suggesting post-transcriptional regulation of VEGFR3 by Notch[48]. Subsequently, it was shown that VEGFR3 endocytosis-dependent activation is mediated by DAB2, the transmembrane protein Ephrin B2, and the cell polarity regulator Par-3 [49]. We have reported that VEGFR3 surface expression and activation in LECs are also regulated by AIP1, a known DAB2-interacting protein (also DAB2IP) [50]. AIP1 enhances both total VEGFR3 and surface VEGFR3 expression without

any effects on the VEGFR3 mRNA. Measurements of the VEGFR3 half-life in LECs by cycloheximide assays show that VEGFR3 half-life changed from 4 h in normal LECs to < 1h in AIP1-deficient LECs, suggesting that AIP1 stabilizes VEGFR3 protein [50]. The effects of AIP1 on VEGFR3 expression and activity correlate with the association of AIP1 with VEGFR3. In contrast, VEGFR2 stability is slightly increased by AIP1 knockdown [31], suggesting that VEGFR2 and VEGFR3 can be differentially regulated in LECs. On the other hand, another endocytic protein epsin could bind to VEGFR3 and mediate the internalization and degradation of VEGFR3, resulting in the termination of VEGFR3 signaling. Therefore, mice with lymphatic epsin-deficiency exhibit increase VEGFR3 protein and dilate lymphatic vessels [41].

In the present study, we aim to examine whether or not the lymphatic system is defective in CCM3-deficient CCM mouse models. We report that mice with an inducible pan-EC deletion (by Cdh5-CreER^{T2}) (*Pdcd10*^{ECKO}) and an inducible LEC-specific deletion of *Ccm3* (*Pdcd10*^{LECKO}) exhibit dilated lymphatic capillaries and collecting vessels with abnormal valve formation. These lymphatic defects resulted from enhanced VEGFR3 transcription and VEGFR3-ER1/2 signaling in CCM3-depleted LECs.

MATREILAS AND METHODS

The authors declare that all supporting data are available within the article or in the Data Supplement or from the corresponding author on request.

Generation of tamoxifen-inducible EC-specific CCM3 deficient mice.

The *Cdh5*-CreER^{T2} mouse line and *Prox1*-CreER^{T2} mouse line was obtained from Dr. Ralf Adams [49] and Dr. Taija Makinen[51], respectively. *Pdcd10*$^{fl/fl}$ mice were crossed with *Cdh5*-CreER^{T2} and *Prox1*-CreER^{T2} mice to generate *Pdcd10*^{ECKO} and *Pdcd10*^{LECKO}, in which CreER^{T2} recombinase expression is driven by the *Cdh5* or the *Prox1* promoter, respectively. For the *in vivo* tamoxifen-induced *Pdcd10* deletion, tamoxifen (Cat# T5648, Sigma-Aldrich, St. Louis, USA) was diluted to 10 mg/mL and fed to mice at a dose of 50 μg/day from P1-P3[52]. For pups, littermates were randomly separated into vehicle (WT) and tamoxifen-fed (*Pdcd10*^{ECKO} or *Pdcd10*^{LECKO}) groups such that the sex ratios of mice in both groups were equal. We extensively analyzed lesions in both male and female pups at P6-P15, and our data showed that sex was not a determinant in lymphatic phenotype. We therefore presented data from combined sexes. Mice were housed under diet from Charles River Laboratory and cared for in accordance with the National Institutes of Health guidelines, and all procedures were approved by the Yale University Animal Care and Use Committee.

Treatment with the VEGFR3 inhibitor or MEK1 inhibitor *in vivo*.

MAZ51 (Cta# M1695, Sigma-Aldrich, St. Louis, USA) or AZD6244 (Selumetinib, Cat# S1008, Selleckchem, TX, USA) was dissolved in 0.5% DMSO at 1 mg/mL. For in vivo experiments, 10 mg/kg MAZ51, AZD6244 or vehicle was intraperitoneally injected into WT or *Pdcd10*^{LECKO} mice from P4 to P14 daily (10 μg/g body weight). Subsequently, mice were analyzed at P15 or P30.

Assessment of basal lymphatic vessel functionality in mouse models.

To determine basal lymphatic vessel function, Evans blue dye (Sigma-Aldrich; 2 mg/mL) was injected intradermally into the mouse foot pads. Tissues were harvested at 30 minutes post-dye injection and Evans blue transported to lymph nodes were measured by extracting the dye with formamide followed by spectrometry assay for absorbance at 610 nm as we previously described[14, 27].

For a lymphatic backflow assay, Fluorescein isothiocyanate (FITC)-dextran (FD2000S; Sigma-Aldrich, St. Louis, MO, USA; 10 μL of 2 mg/mL in Saline) was injected into mouse mesentery lymph nodes. The FITC-dextran labeled mesentery lymph nodes and their lymphatic vessels were imaged using a CCD camera on a stereo Epi-Fluorescence microscope (Leica) at various times (0 - 30 minutes) post-injection. Mean fluorescence intensity (MFI) of FITC-Dextran was quantified by Image J as we previously described[30].

Fluorescent whole-mount staining.

Fluorescent whole-mount staining was performed as we previously described[14, 27, 30]. Mouse tissues were collected at various ages and then fixed in 4% PFA for 2 hours on ice. Tissues were permeabilized in 0.5%Triton/PBS (5% normal donkey serum) overnight at 4°C, followed by incubation with primary antibodies diluted 1:100 in 0.1% Triton/PBS (1% normal donkey serum) overnight at 4°C. The following day, retinas were washed in PBS and then incubated with fluorescein-conjugated primary antibodies against CD31, VEGFR3, Prox1 and/or SMA overnight at 4°C. Tissues were then washed five times with PBS and mounted by making four incisions in the fluorescent mounting medium. Pictures were taken with the same exposure and gain settings using a confocal Zeiss Airyscan 880 microscope (Zeiss, Germany). Vascular areas were outlined using NIH Image J software and quantified as the percentage of the total area of the retina analyzed.

Immunofluorescence analysis for tissue sections.

Tissue section staining was performed as we previously described[14, 27, 30]. Mouse tissues were harvested, fixed with 4% paraformaldehyde (PFA), embedded in OCT, and sectioned into 5-μm thick sections. Slides were washed with PBS twice to remove OCT and then blocked in 5% donkey serum in 0.3% TritonX-100 in PBS for 30 minutes to prevent non-specific staining and to permeabilize the tissues. Slides were then incubated with primary antibodies against CD31, VEGFR3, Prox1 and/or SMA overnight at 4°C. The next day, slides were washed with PBS three times and then incubated with secondary antibodies (1:400) at room temperature for one hour. After washing in PBS three more times, slides were mounted with VECTASHIELD mounting medium with DAPI (Vector Laboratory). Images were taken under a confocal Leica SP8 STED microscope (Leica, Germany).

For cultured cells, HDLECs were fixed in 4% PFA for 20 minutes, washed with PBS, and permeabilized with 0.1% TritonX-100 for 2 minutes. After blocking for 30 minutes, primary and secondary antibodies were applied sequentially. Images were taken under a confocal Leica SP5 microscope (Leica, Germany).

Gene expression.

Total RNA was isolated from tissues using the RNeasy kit with DNase I digestion (Qiagen, Valencia, CA). Reverse transcription was performed using standard procedures (Super Script first-strand synthesis system; Qiagen) with 1 μg of total RNA. Quantitative real-time polymerase chain reaction (qPCR) was performed using iQ SYBR Green Supermix on an iCycler real-time detection system (Bio-Rad Laboratories, Inc., Hercules, CA). qRT-PCR with specific primers (e.g., CCM3, VEGFR2, VEGFR3 and P65) was performed.

Cell Culture, transfection and growth factors.

Clonetics™ human dermal lymphatic microvascular ECs (HMVEC-dLys Neo or HDLECs in our presentation) isolated from neonatal foreskin were purchased from Lonza Walkersville, Inc (Cat# CC-2812, Walkersville, MD, USA), and were grown in Microvascular Endothelial Cell Growth Medium-2 MV (EGM2) (Lonza). HDLECs were verified by positive staining for lymphatic endothelial cell (LEC) markers VEGFR3, Prox1 and podoplanin.

SVEC4–10, a lymphatic endothelial cell line derived by SV40 (strain 4A) transformation of endothelial cells from axillary lymph node vessels, was purchased from ATCC (CRL-2181). Cells were cultured in DMEM media with 10% FBS. 293T cells were transfected with VEGFR3 plasmid[47, 53] with Lipofectamine 2000 according to the manufacturer's instructions (Invitrogen).

Human recombinant VEGF-C were from R&D Systems Inc. (Minneapolis, MN) and used at 10 ng/mL. Small interfering RNAs (siRNAs) were purchased from Santa Cruz Biotechnology (Santa Cruz, CA, USA): CCM3 siRNA (h) (sc-62084), CCM3 siRNA (m) (sc-62085), NF-κB P65 siRNA (h) (sc-29410), NF-κB P65 siRNA (m) (sc-29411), VEGFR2 siRNA (h) (sc-29318), VEGFR2 siRNA (m) (sc-35390), VEGFR3 siRNA (h) (sc-35397), VEGFR3 siRNA (m) (sc-35398), karyopherin alpha 2 (KPNA2) siRNA (h) (sc-35741). siRNAs (20 μM) were transfected into cells by Oligofectamine (Life Technologies, Inc.; Invitrogen), following protocols provided by the manufacturer (Invitrogen). At 48 hours post-transfection, cells were harvested for protein analysis.

For inhibitor experiments, cells were treated by various inhibitors, including VEGFR3 inhibitor MAZ51 (10 μM), VEGFR2 inhibitor SU5402 (10 μM), ERK1/2 upstream MEK1 inhibitor AZD6244 (10 μM) or Angiopoietin-2 neutralization antibody (10 ng/ml). Cells were pretreated with inhibitors for 4 hours, followed by VEGF-C (10 ng/mL) stimulation for 5 minutes.

EdU incorporation assays.

For EdU incorporation assay in vitro, cells were incubated with 10 μM 5-ethynyl-2′-deoxyuridine (EdU) for 4 h prior to fixation with 4% PFA for 30 minutes at room temperature. Once fixed, cells were subjected to EdU assays using the Click-iT EdU kits (ThermoFisher Scientific).

Protein extraction and western blot analysis.

Freshly dissected unfixed tissue was homogenized in lysis buffer. The lysates were centrifuged at 13000g for 10 minutes at 4°C. Supernatants were collected and determined with a Bradford Protein Assay kit (Bio-Rad, Hercules, CA). The cell lysates were subjected to SDS-PAGE followed by immunoblotting (Immobilon P; Millipore, Milford, MA) with specific antibodies followed by detection using an enhanced chemiluminescence kit (Amersham Life Science, Arlington Heights, IL).

Study Design and Statistical Analysis.

Group sizes were determined by an a priori power analysis for a 2-tailed, 2-sample Student *t* test with an α of 0.05 and power of 0.8, to detect a 10% difference in lesion size at the end point. Animals were grouped with no blinding but randomized during the experiments. Male and female animals were used in equal numbers for all experiments. No samples or animals were excluded from analysis. All quantifications (lesion sizes, junctional integrity, sprout length and lumen) were performed in a blind fashion. All figures are representative of at least 3 experiments unless otherwise noted. All graphs report mean ± standard error of mean (SEM) values of biological replicates. The normality and variance were not tested to determine whether the applied parametric tests were appropriate. Comparisons between two groups were performed by unpaired, 2 tailed Student *t* test, between >2 groups by 1-way ANOVA followed by Bonferroni post hoc or by 2-way ANOVA followed by Bonferroni's post hoc using Prism 6.0 software (GraphPad). *P* values were 2-tailed and values <0.05 were considered to indicate statistical significance. $P<0.05$, $P<0.01$ and $P<0.001$ are designated in all figures with *, **, ***, respectively.

DATA AVAILABILITY STATEMENT:

All data, including data associated with main figures and Supplemental figures, are available within the article or in the online-only Data Supplement or from the corresponding author on request. Source data are provided with this paper.

RESULTS

Inducible EC-specific *Ccm3* deletion (*Pdcd10*^{ECKO}) causes defects in both blood and lymphatic vessels in various organs.

We previously created inducible pan-EC *Pdcd10* knockout mice (*Pdcd10*^{ECKO}) using the Cdh5-CreER^{T2} line [49]. Upon tamoxifen feeding of pups at postnatal days (P) 1–3, *Pdcd10*^{ECKO} pups develop severe CCM lesions in the brain and retina by P10 and do not survive beyond P15 [27, 30]. Examining organ structures and morphologies revealed that *Pdcd10*^{ECKO} pups had severe vascular damage in the brain, retina, and spleen [30] (Supplemental Fig. I A-C). We also observed hemorrhages in other organs, including the intestine and lymph nodes (LNs) (Supplemental Fig. I D-E). Interestingly, we observed that *Pdcd10*^{ECKO} mice exhibited chyle fistula, i.e., chyle blood in the thoracic (pleural) and chyle ascites (milky peritoneal cavity) (Fig. 1A).

We then examined lymphatic vessels in the *Pdcd10*^{ECKO} mice. Imaging of perfused mesentery tissues showed blood-filled lymphatics in *Pdcd10*^{ECKO} mice (Fig. 1B), consistent with leaky blood vessels in these mice. Whole-mount staining of collecting lymphatic vessels in the mesentery showed that pan-EC deletion of *Ccm3* caused enlarged and irregular lymphatic vessels (Fig. 1C). Of interest, collecting lymphatic vessels were abnormally patterned, with alternating areas of vessel ectasia and constrictions, a phenotype that has been observed in *Foxc2*-deficient mice [54]. Quantitative analyses showed that *Ccm3* deletion significantly reduced the percentages of V-shaped valve numbers (Fig. 1D) and induced enlargement of the lumen in the collecting lymphatic vessels (Fig. 1E). Immunostaining of intestinal wall and villi with CD31 and VEGFR3 indicated that both blood capillaries and lymphatic capillaries (called lacteal in villi) were dilated in *Pdcd10*^{ECKO} mice compared to wildtype (WT) (Fig. 1F-K). Together these observations suggest that mice with inducible pan-EC *Ccm3* deletion (*Pdcd10*^{ECKO}) exhibit blood vascular leakage and lymphatic defects in various organs.

Inducible *Ccm3* deletion in lymphatic EC (*Pdcd10*^{LECKO}) induces lymphatic dysfunction without blood vascular leakage.

To specifically define the role of CCM3 in LECs, we generated inducible LEC-specific *Ccm3* knockout mice (*Pdcd10*^{LECKO}) by crossing *Pdcd10*$^{lox/lox}$ with *Prox1*-CreER^{T2} mice[51]. In contrast to *Pdcd10*^{ECKO} mice, *Pdcd10*^{LECKO} mice did not die perinatally, as did *Pdcd10*^{ECKO} mice, and *Pdcd10*^{LECKO} mice survived up to 2 months. *Pdcd10*^{LECKO} mice did not exhibit CCM lesions in the brain, and no blood-filled mesenteries were detected (Supplemental Fig. II). Of note, *Pdcd10*^{LECKO} mice had reduced fat tissues surrounding the mesentery compared to WT mice, highlighting the role of lymphatics in adipose and lipid metabolism [55, 56].

We directly measured lymphatic function by dye uptake assays. Tail vein injection of Evans blue dye (EBD) followed by visualization of EBD uptake in the sciatic and iliac LNs detected strong EBD deposition in WT mice. However, EBD uptake in both ischiatic and lumbar LNs was significantly reduced in *Pdcd10*^{LECKO} mice compared to WT mice (Fig. 2A with quantifications in 2B-C), indicating attenuated lymphatic function in *Pdcd10*^{LECKO} mice. Lymphatic drainage was further measured by injecting FITC-dextran into the mesentery LNs. As expected, FITC-dextran was transported to the thoracic ducts in WT mice without backflow. In contrast, *Pdcd10*^{LECKO} mice had dye outflow in multiple afferent collecting lymphatic vessel branches, indicating lymph backflow (Fig. 2D-E).

Lymphatic vessels were then visualized by co-immunostaining with various markers, including CD31, VEGFR3, and LYVE1. Immunostaining of lumbar LNs indicated that CD31^{+}VEGFR3^{+}LYVE^{+} but SMA^{-} lymphatic capillaries were dilated in *Pdcd10*^{ECKO} mice compared to WT (Fig. 2F-G). Whole-mount staining of mesentery tissues with CD31 and VEGFR3 indicated that lymphatic vessels were drastically enlarged with non-V-shape valves in *Pdcd10*^{LECKO} mice compared to those in WT mice (Fig. 2H-J). Further staining with CD31 and SMA distinguished aortas, veins, and lymphatics with strong, moderate, and weak SMA staining, respectively (Fig. 2K). Quantifications indicated that lymphatics, but not aortas or veins, were significantly enlarged in *Pdcd10*^{LECKO} mice (Fig. 2L). Consistent with

reduced-fat tissues surrounding the mesentery in *Pdcd10*^{LECKO} mice, a reduced capillary network in the mesentery was observed.

Pdcd10^{LECKO} mice exhibit lymphatic hyperplasia with increased VEGFR3-ERK1/2 signaling.

Recent studies suggest that dilated blood capillaries in CCM result from hyper-proliferation [57, 58]. To determine if dilated lymphatics contained more LECs, mesentery tissues were whole-mount stained with CD31 and Prox1 to visualize LEC nuclei. The number of lymphatic branches was increased in *Pdcd10*^{LECKO} mice compared to WT mice as visualized by Prox1^{+} vessels. Moreover, Prox1^{+} LECs per vessel and Prox1^{+} cells per vascular area (mm^{2}) were also significantly increased in *Pdcd10*^{LECKO} mice (Fig. 3A-C). These analyses suggest that *Pdcd10*^{LECKO} exhibited lymphatic hyperplasia.

VEGFR3 expression and activity have been closely associated with lymphatic growth and maturation. Deletion of VEGFR3 induces lymphatic hypoplasia, whereas increased VEGFR3 expression/activity causes lymphatic hyperplasia [40, 41]. Therefore, we examined VEGFR3 expression and activation in *Pdcd10*^{LECKO} mice. Although phosphorylation of both VEGFR2 and VEGFR3 increased in the *Pdcd10*^{LECKO} mesentery tissues, only the total VEGFR3 protein level was significantly upregulated. Interestingly, phosphorylation of ERK1/2, but not p-Akt, was increased in *Pdcd10*^{LECKO} mesentery tissues (Fig. 3D). Moreover, VEGFR3-ERK1/2 signaling was upregulated in the mesentery and spleen but not in the retina tissues (Fig. 3E), suggesting the increased VEGFR3-ERK1/2 signaling could be VEGFR3^{+} lymphatics-specific. We further detected co-staining of p-ERK1/2 with VEGFR3 in the lymphatic vessels of mesentery tissue and lumbar LNs (Fig. 3F-G with quantifications in 3H-I). These data indicate that *Pdcd10*^{LECKO} mice exhibit lymphatic hyperplasia with increased VEGFR3-ERK1/2 signaling.

Regulation of VEGFR3 signaling regulation in lymphatic ECs.

In vivo data suggested that VEGFR3 expression and VEGFR3-ERK1/2 signaling were increased in lymphatic vessels. To determine if this is LEC-autonomous, we examined the effects of CCM3 silencing on VEGFR3 signaling in cultured human dermal microvascular lymphatic ECs (HDLECs)[47, 53]. Consistent with the in vivo observations, expression of VEGFR3, but not VEGFR2, was increased by CCM3 silencing. VEGF-C induces phosphorylation of VEGFR3 at Y1063/68 within the kinase activation loop essential for VEGFR3 kinase activity [59, 60]. siCCM3 enhanced p-VEGFR3 and p-ERK1/2 but not p-VEGFR2 or p-Akt in LECs (Fig. 4A). To determine if the VEGFR3-ERK1/2 signaling is responsible for the lymphatic hyperplasia observed in vivo, we tested the effect of inhibition of VEGFR3/ERK1/2 on HDLEC proliferation in vitro. Silencing of CCM3 augmented LEC proliferation as determined by an EdU incorporation assay. Inhibition of VEGFR3 or ERK1/2, but not of VEGFR2 or Angpt2, attenuated CCM3 silencing-induced LEC proliferation (Fig. 4B-C). Much weak effects of these inhibitors were observed on the proliferation of controls cells (Supplemental Fig. III). These data suggest that augmented VEGFR3-ERK1/2 signaling is critical for increased LEC proliferation by the CCM3 deletion. Previous reports suggest that VEGFR3 homodimer activates ERK1/2, while VEGFR2/VEGFR3 heterodimer preferentially activates Akt [48, 61, 62]. We reasoned that

increased VEGFR3 abundance and the resulting increase in the VEGFR3/VEGFR2 ratio in LECs could be responsible for enhanced ERK1/2 signaling, and silencing VEGFR2 would enhance ERK1/2 activation in LECs. Indeed, silencing of VEGFR2 by siRNA, but not inhibition of VEGFR2 kinase by a pharmacological inhibitor, augmented VEGF-C-induced p-VEGFR3 and p-ERK1/2 in both siCtrl and siCCM3 LECs (Fig. 4D). These data indicated that the VEGFR3 abundance or VEGFR3/VEGFR2 ratio determines ERK1/2 signaling in LECs.

We compared expression of VEGFR2 and VEGFR3 between HDLEC and SVEC4-10, a mouse LEC line. While HDLEC expressed both VEGFR2 and VEGFR3, SVEC4-10 expressed more VEGFR3 protein but lacked VEGFR2 protein expression compared to HDLECs. Moreover, the three bands of VEGFR3 (195, 175, and 135 kDa) [48] were more readily detected in SVEC4-10 than HDLEC (Fig. 4E), providing a better system to investigate the role of CCM3 in VEGFR3 signaling. Silencing of Ccm3 in SVEC4-10 increased both mRNA and protein levels of VEGFR3 (Fig. 4E-H). We also examined the half-life ($t_{1/2}$) of VEGFR3 in ECs in the presence of the protein synthesis inhibitor cycloheximide. Notably, the top two bands (175 and 159 kDa) of VEGFR3 were very unstable, and the $t_{1/2}$ was ~20 min, similar to VEGFR2, as we previously reported [50]. In contrast, the 135 kDa band was relatively stable with a $t_{1/2}$ of ~9 h. Importantly, the Ccm3 deletion had no effect on the stability of the three VEGFR3 bands compared to the control cells (Fig. 4I-J). Similar to the results observed in lymphatic vessels and HDLECs, ERK1/2 but not Akt was augmented in siCCM3 SVEC4-10 (Fig. 4K). Moreover, the silencing of CCM3 drastically increased phosphorylation of all three VEGFR3 bands due to increased VEGFR3 expression, as the ratio of p-VEGFR3:VEGFR3 was similar between the control and CCM3-depleted cells (Fig. 4K). Altogether, our data suggest that VEGFR3 expression in LECs is primarily regulated at the transcriptional level.

CCM3 regulates NF-κB nuclear translocation and NF-κB-dependent VEGFR3 transcription in LEC.

Because VEGFR3 expression in LECs is primarily regulated at the transcriptional level, we determined potential transcriptional factor(s) responsible for VEGFR3 expression. Transcriptional factors, including Notch, Prox1, and NF-κB, are known to regulate VEGFR3 expression [43-45]. We first examined the expression and activation of these transcriptional factors in the lymphatic tissues. Among these, only NF-κB activation, as determined by phosphorylation of P65 (p-P65), peaked at P5 as VEGFR3 expression increased in Ccm3-deficient mice. IκBα, an inhibitor of NF-κB signaling, was at lower levels at P15 compared to P5 and P30, correcting the NF-κB activity. However, there was no differences between WT and *Ccm*3-deficient mice (Fig. 5A). Notch activation detected by cleaved Notch and expression of Prox1 were on at P5 and peaked at P15 (Fig. 5A), likely reflecting increased lymphatic vessels. Moreover, the mRNA level of Vegf3, but not of Vegfr2 or P65, was increased by Ccm3 deficiency in mesentery tissues (Supplemental Fig. IV A). Because the kinetics of NF-κB activity and VEGFR3 expression were tightly correlated, we further investigated if P65 was required for CCM3-deletion-induced VEGFR3 mRNA expression. To this end, HDLECs were silenced with siCCM3 in the absence or presence of P65 siRNAs, and VEGFR3 mRNA and protein were determined by qRT-PCR and Western

blotting. siCCM3-induced upregulation of VEGFR3 mRNA (Supplemental Fig. IV B) and protein was diminished by P65 siRNA (Fig. 5B). We then determined how CCM3 depletion augmented NF-κB signaling. Silencing of CCM3 in HDLECs enhanced basal and LPS-induced p-P65 without obvious effects on the total levels of P65 and P50. Of note, siCCM3 did not alter basal or LPS-induced IκBα degradation (Fig. 5C).

To determine whether the observed lymphatic phenotypes reflect loss of CCM complex function or loss of CCM3-specific function, we compared knockdown of CCM1 (KRIT1) or CCM2 to that for CCM3 on the VEGFR3 expression in lymphatic ECs. Our results indicated that silencing of CCM3 increased VEGFR3 expression and VEGF-C-induced VEGFR3 phosphorylation in human LECs. Interestingly, silencing of CCM2, but not of CCM1, also increased VEGFR3 expression and activity. In contrast, silencing of CCM1, CCM2 or CCM3 reduced VEGFR2 expression (Supplemental Fig. V A). Since CCM2 and CCM3 form complex in ECs [22, 23], we tested if CCM2 knockdown also affected the NF-κB signaling. While silencing of CCM3 augmented LPS-induced P65 phosphorylation without effects on IκBα degradation, knockdown of CCM2 had no such effects (Supplemental Fig. V B). These data indicate that CCM3 specifically regulates the NF-κB-VEGFR3 axis in LECs.

IκBα is a protein inhibitor associated with P65 in the cytosol and prevents P65 nuclear translocation; IκBα phosphorylation and degradation release P65 followed by P65 nuclear translocation and phosphorylation by specific kinases[63]. We examined if CCM3 deletion affected P65 nuclear translocation by detecting P65 in the cytosolic and nuclear fractions. Silencing of CCM3 in HDLECs increased nuclear accumulation of P65 protein at basal and at 5-15 min post-LPS treatment compared to siCtrl cells. Nuclear protein upstream stimulating factor-2 (USF-2) was not altered by CCM3 depletion (Fig. 5D). Notably, CCM3 could be detected in both the cytosol and nucleus as previously reported [64]. These data suggested that CCM3 depletion in HDLECs facilitated P65 nuclear translocation. To define the mechanism by which CCM3 restrained P65 nuclear translocation, we searched for CCM3-associated proteins in Flag-CCM3 stable expression HeLa cells; CCM3-associated proteins were separated using an anti-Flag column followed by mass-spectrometry. Among 10 prominent proteins detected in the mass-spectrometry, 6 were nuclear/nuclear membrane proteins, including nucleophosmin, spindlin-1, spindlin-2, and importin alpha-subunit (aka KPNA2). Importin alpha subunits bind specifically and directly to substrates containing either a simple or bipartite nuclear localization signal (NLS) motif. KPNA2 together with importin beta-subunit dock substrates to the nuclear pore complex (NPC) for subsequent nuclear translocation [65]. Among the six members of the importin alpha family, it has been shown that KPNA2 is pivotal to the P65 nuclear import[64]. Therefore, we investigated if CCM3-KPNA2 association regulated NF-κB activation. We hypothesized that CCM3, by binding to KPNA, regulates KPNA-mediated NF-κB nuclear translocation and NF-κB-dependent gene expression. We first confirmed the CCM3-KPNA2 interaction in HDLECs by co-immunoprecipitation assays. Association of CCM3 with KPNA2 in HDLEC was evident under basal conditions, and this association gradually declined upon LPS stimulation. KPNA2 was not detected in immunoprecipitations of lysates from the CCM3-knockdown cells (Fig. 5E). We then examined how CCM3 regulated KPNA2-P65 interactions. An association between PKNA2 and P65 in siCtrl cells was not detected under

the basal condition and was induced upon LPS stimulation at 15 min followed by a decline at 30 min. In contrast, the KPNA2-P65 complex was readily formed at basal followed by a decline upon LPS treatment, suggesting that CCM3 deletion enhanced the KPNA2-P65 complex formation (Fig. 5F). Indeed, nuclear P65 was increased in response to LPS in control cells. However, silencing of KPNA2 drastically diminished the LPS-induced p65 nuclear translocation (Fig. 5G), highlighting the critical role of KPNA2 for P65 nuclear import. Finally, we determined the functional significance of KPNA2 in CCM3 deletion-induced VEGFR3 expression. To this end, CCM3 in HDLECs was silenced by siRNA in the absence or presence of siKPNA2. VEGFR3 was upregulated by CCM3 silencing, but this upregulation of VEGFR3 was diminished by co-silencing of KPNA2 (Fig. 5H). Together, these data suggest that CCM3 associates with KPNA2 in control cells to prevent the binding of KPNA2 to P65, and CCM3 depletion frees PKNA2 for the P65 interaction, leading to enhanced P65 nuclear import and subsequent VEGFR3 transcription.

Inhibition of VEGFR3-ERK1/2 signaling rescues the lymphatic hyperplasia in *Pdcd10*^{LECKO} mice.

To determine if inhibition of VEGFR3-ERK1/2 could rescue lymphatic dysfunction in *Pdcd10*^{BECKO} mice, we tested the effects of specific inhibitors of VEGFR3 and ERK1/2 in the mouse models. To this end, we intraperitoneally injected VEGFR3-specific inhibitor MAZ51 into WT and *Pdcd10*^{LECKO} mice at 5 μg/g body weight daily from P2-P14 and mesentery tissues were harvested at P15 (Fig. 6A for MAZ protocol). MAZ attenuated p-VEGFR3 and its downstream signaling without effects on p-VEGFR2 (Fig. 6B). Whole-mount staining of mesentery tissues with CD31 with VEGFR3 showed that MAZ had no evident effect on WT lymphatics. However, MAZ drastically reversed the dilated lymphatic vessels with flat-shape valves in *Pdcd10*^{LECKO} mice to normal lymphatics with V-shape valves (Fig. 6C-D). Similar rescue effects were observed with AZD6244, an inhibitor specific to the ERK1/2 upstream activator MEK1, on mesentery lymphatics (Supplemental Fig. VI). Furthermore, MAZ diminished lymphatic hyperplasia in mesentery tissues as measured by whole-mount staining with CD31 and Prox1, as evident by attenuated Prox1^{+} LEC/lymphatic vessel and Prox1^{+} cells/lymphatic vessel area (mm^{2}) upon MAZ treatment in *Pdcd10*^{LECKO} mice (Fig. 6E-F). These analyses suggest that MAZ diminished the lymphatic hyperplasia in *Pdcd10*^{LECKO} mice.

We then determined if MAZ normalized lymphatic function in *Pdcd10*^{LECKO} mice by dye uptake/transport assays. Tail vein injection of EBD followed by visualization of EBD uptake in the sciatic LN detected strong EVB deposition in WT mice, and MAZ had no effects on EBD uptake. While EBD uptake was not detected in *Pdcd10*^{LECKO} mice, MAZ significantly increased EBD accumulation in the sciatic LN (Fig. 6G-H). Injection of FITC-dextran into the mesentery LN followed by fluorescence imaging indicated that untreated and MAZ-treated WT mice had no backflow. *Pdcd10*^{LECKO} mice exhibited lymph backflow as indicated by dye outflow in multiple afferent collecting lymphatic vessel branches, and MAZ significantly attenuated the backflow (Fig. 6I-J). These data suggest that increased VEGFR3-ERK1/2 signaling contributes to the lymphatic hyperplasia in *Pdcd10*^{LECKO} mice.

DISCUSSION

The role of CCM3 in VEGFR3 signaling and lymphangiogenesis has not been investigated. Here we report that mice with an inducible deletion of *Ccm3,* specifically in LECs (*Pdcd10*^{LECKO}), exhibited enlarged lymphatic capillaries and dilated collecting vessels with malformed valve structure. In vivo, functional assays indicate that lymphatic vessels in *Pdcd10*^{LECKO} mice are defective in drainage. Our in vivo and in vitro analyses suggest that VEGFR3 expression, and therefore VEGFR3-ERK1/2 signaling, are drastically increased and sustained in the *Pdcd10*^{LECKO} lymphatics. CCM3, by binding to the NF-κB P65 nuclear import regulator KPNA2, regulates NF-κB activation and NF-κB-dependent VEGFR3 transcription in LECs; loss of CCM3 releases KPNA2 and augments NF-κB P65 nuclear translocation and VEGFR3 transcription, leading to lymphatic ectasia and dysfunction. More importantly, pharmacological inhibition of VEGFR3-ERK1/2 signaling normalizes lymphatic structure and ameliorates lymphatic vessel dysfunction in *Pdcd10*^{LECKO} mice. Our study uncovers a novel function of CCM3 in VEGFR3 signaling and lymphangiogenesis (Fig. 7: A model for CCM3 regulated VEGFR3 expression and lymphatic function).

Distinct from these previous findings on VEGFR3 regulation, our current study has uncovered a novel mechanism for VEGFR3 regulation at a transcriptional level without effects on intracellular trafficking or the protein stability of VEGFR3. In particular, our study defines a novel mechanism by which CCM3 regulates NF-κB signaling and NF-κB-mediated VEGFR3 transcription in LECs. By examining expression and activation of the critical transcriptional factors for VEGFR3 expression in the lymphatic tissues, we found that increased VEGFR3 expression coincides with the kinetics of NF-κB activation in *Pdcd10*^{LECKO} mice; NF-κB activation precedes increased Notch activation and Prox1 expression in lymphatics. Moreover, silencing of NF-κB P65 diminished the augmented VEGFR3 mRNA expression in CCM3-deficient LECs. We provide four pieces of strong evidence that CCM3 controls the nuclear import of NF-κB P65 in the regulation of VEGFR3 expression. 1) Silencing of CCM3 does not alter basal or LPS-induced IκBα phosphorylation and degradation, a process that precedes the P65 nuclear translocation and gene transcriptions. 2) Silencing of CCM3 in LECs enhances both basal and LPS-induced nuclear accumulation and phosphorylation of NF-κB P65. 3) By mass-spectrometry, we identified a new CCM3-binding partner importin alpha-1 subunit (aka KPNA2), a critical factor for P65 nuclear translocation [64]. We show that CCM3 normally associates with KPNA2 in HDLECs, but CCM3 depletion releases KPNA2 to facilitate KPNA2-P65 interactions and P65 nuclear transport under basal conditions and in response to LPS. 4) Silencing of KPNA2 drastically attenuates P65 nuclear translocation and VEGFR3 expression in LECs. Altogether, our study supports the model that CCM3 restrains P65 nuclear import by interaction with KPNA2, and CCM3 loss facilitates P65 nuclear translocation and subsequent VEGFR3 expression (Fig. 7). Of clinical relevance, it is known that circulating LPS from gram-negative bacteria, via binding to its receptor TLR4 on the brain endothelium, accelerates the growth of CCM lesions in the brain of *Pdcd10*^{ECKO} mice[28, 66]. It will be interesting to explore if LPS from gram-negative bacteria that reside in the gut microbiome augments NF-κB-dependent VEGFR3 expression in lymphatic

endothelium and aggravates the lymphatic defects of Ccm3-deficient mice. By comparing knockdown of CCM1 (KRIT1) or CCM2 to that for CCM3 on the NF-κB-VEGFR3 signaling in lymphatic ECs, our data indicate that CCM3 specifically regulates the NF-κB-VEGFR3 axis. Although in vitro silencing of CCM2 increases VEGFR3 expression in LECs, it needs to further determine how CCM2 regulates VEGFR3 expression, and more importantly the lymphatic phenotype in *Ccm2*-deficient mice.

All three forms of VEGFR3 (195-, 175- and 135-kDa) increased upon CCM3 depletion in LECs. We observed that all three VEGFR3 forms are glycosylated and can be phosphorylated in response to VEGF-C. However, they are differentially regulated in response to VEGF-C. Specifically, both the 195 kDa and the 135 kDa (but not the 175 kDa) forms are localized on the LEC membrane and undergo endocytosis in response to VEGF-C. Of note, the glycosylation, membrane localization, and VEGF-C induced intracellular trafficking of VEGFR3 are not altered by CCM3 depletion in LECs. However, CCM3 loss shifts VEGFR3 toward the ERK1/2 axis from the Akt axis. VEGF-C strongly induces activation of VEGFR3 and downstream Akt signaling with weak ERK1/2 activation [53]. It has been proposed that VEGFR2/VEGFR3 heterodimers present in LECs preferentially activate Akt while VEGFR3 homodimers activate ERK1/2 in LECs [62]. Our data support the model that VEGFR3 abundance and the VEGFR3/VEGFR2 ratio in the LECs determines the outcome of VEGF-C-VEGFR3 signaling. First, silencing of CCM3 in human LECs increases VEGFR3 expression and thus strongly augments both basal and VEGF-C-induced ERK1/2 activation without evident effects on Akt. Second, silencing of VEGFR2 in HDLECs enhances VEGF-C-induced ERK1/2 activation. Third, the lymphatic cell line SVEC4-10, which has much higher VEGFR3 and lower VEGFR2 expression (thus with a higher VEGFR3/VEGFR2 ratio) compared to HDLECs, exhibits readily detectable ERK1/2 signaling in response to VEGF-C. The exact mechanism by which VEGFR3 activates ERK1/2 is not completely understood in part due to the lack of identified adaptor proteins directly linking VEGFR3 to ERK1/2 activation, despite Shc/GRB2 being implicated in both ERK1/2 and Akt activation [59, 60]. Five phosphotyrosine sites have been identified on VEGFR3 in response to VEGF-C. However, only three of the five sites were detected on VEGFR3 upon formation of VEGFR3/VEGFR2 heterodimers with the two most carboxyl-terminal tyrosine residues inaccessible to the VEGFR2 kinase [48, 61]. It is plausible that these two most C-terminal phosphotyrosine residues are critical for ERK1/2 signaling with yet-to-be-identified adaptors. We have previously shown that bone marrow tyrosine kinase on chromosome X (BMX) binds to and directly phosphorylates VEGFR3 at the C-terminal tail outside the kinase domain for PI3K recruitment, leading to PI3K-Akt signaling. Silencing of BMX reveals complete inhibition of VEGF-C induced Akt activation [53]. One possible model is that CCM3 deletion, by increasing VEGFR3 abundance and also therefore VEGFR3 homodimers, reduces the recruitment of Akt-activating adaptors (such as BMX) while augmenting the binding of ERK1/2-activating adaptors to VEGFR3, leading to increased EKR1/2 signaling.

Of clinical relevance, the lack of increased PI3-Akt signaling by loss of CCM3 is consistent with recent reports that CCM lesion progression needs additional activated PI3K-Akt signaling [12]. In humans and mouse models, CCM loss-of-function (LOF) mutation and PI3KAC gain-of-function (GOF) mutations exhibit synergistic effects in CCM lesion

formation[12]. However, the imbalanced VEGFR3 toward ERK1/2 signaling appears to be sufficient to induce LEC proliferation and the lymphatic ectasia observed in our study. ERK1/2 has been implicated in LEC junctional organization and lymphatic permeability [67, 68]. Consistently, we show that inhibition of ERK1/2 attenuates LEC hyperproliferation in vitro and hyperplasia in the *Pdcd10*^{LECKO} mouse models, supporting that ERK1/2-mediated effects contribute to the lymphatic phenotype observed in the *Pdcd10*^{LECKO} mice. Thus far, there is no clinical reports on lymphatic defects in CCM3 disease patients. However, our current study warrants further detailed analyses on the edema and potential lymphatic dysfunction in the CCM patients.

Supplementary Material

Refer to Web version on PubMed Central for supplementary material.

Acknowledgments:

We thank Al Mennone for his help acquiring images at the Yale University Center for Cellular and Molecular Imaging (CCMI). We also thank the Yale University CCMI Electron Microscopy Core Facility. The sequencing service was conducted at the Yale Stem Cell Center Genomics Core facility and was supported by the Connecticut Regenerative Medicine Research Fund.

a) Sources of Funding:

This work was partly supported by NIH grants HL157019, and National Career Development Award from American Heart Association 19CDA34760284 (HJZ).

NON-STANDARD ABBREVIATIONS:

CCM	cerebral cavernous malformation
CNS	central nervous system
DAPI	4′,6-diamidino-2-phenylindole
CSPG4	chondroitin sulfate proteoglycan 4
EBD	Evans blue dye
EC	endothelial cell
FITC-dextran	fluorescein isothiocyanate-dextran
HBMVEC	human dermal microvascular ECs
H&E	hematoxylin and eosin
KO	knockout
KRIT1	Krev/Rap1 Interacting Trapped 1
LEC	lymphatic endothelial cell
LN	lymph node

OSM	osmosensing scaffold for mitogen-activated protein kinase kinase-3
P	postnatal day
PBS	phosphate-buffered saline
PDCD10	programmed cell death 10
PFA	paraformaldehyde
PE	phenylephrine
siRNA	small interfering RNA
SMA	smooth muscle cell actin
SMC	smooth muscle cells
VEGF	Vascular endothelial growth factor
VEGFR3	VEGF receptor-3
WT	wildtype

REFERENCES

1. Otten P, Pizzolato GP, Rilliet B and Berney J. [131 cases of cavernous angioma (cavernomas) of the CNS, discovered by retrospective analysis of 24,535 autopsies]. Neurochirurgie. 1989;35:82–3, 128-31. [PubMed: 2674753]
2. Rigamonti D, Hadley MN, Drayer BP, Johnson PC, Hoenig-Rigamonti K, Knight JT and Spetzler RF. Cerebral cavernous malformations. Incidence and familial occurrence. N Engl J Med. 1988;319:343–7. [PubMed: 3393196]
3. Revencu N and Vikkula M. Cerebral cavernous malformation: new molecular and clinical insights. J Med Genet. 2006;43:716–21. [PubMed: 16571644]
4. Akers A, Al-Shahi Salman R, Awad IA, et al. Synopsis of Guidelines for the Clinical Management of Cerebral Cavernous Malformations: Consensus Recommendations Based on Systematic Literature Review by the Angioma Alliance Scientific Advisory Board Clinical Experts Panel. Neurosurgery. 2017;80:665–680. [PubMed: 28387823]
5. Ardeshiri A, Ardeshiri A, Beiras-Fernandez A, Steinlein OK and Winkler PA. Multiple cerebral cavernous malformations associated with extracranial mesenchymal anomalies. Neurosurg Rev. 2008;31:11–7; discussion 17-8. [PubMed: 17957396]
6. Ma L, Zhang S, Li Z, Wu CX, Wang Z, Zhan L, Hao Q, Wang H, Ye X, Chen X, Liu YO, Wang S and Zhao YL. Morbidity After Symptomatic Hemorrhage of Cerebral Cavernous Malformation: A Nomogram Approach to Risk Assessment. Stroke. 2020;51:2997–3006. [PubMed: 32951540]
7. Sahoo T, Johnson EW, Thomas JW, et al. Mutations in the gene encoding KRIT1, a Krev-1/rap1a binding protein, cause cerebral cavernous malformations (CCM1). Hum Mol Genet. 1999;8:2325–33. [PubMed: 10545614]
8. Liquori CL, Berg MJ, Siegel AM, et al. Mutations in a gene encoding a novel protein containing a phosphotyrosine-binding domain cause type 2 cerebral cavernous malformations. Am J Hum Genet. 2003;73:1459–64. [PubMed: 14624391]
9. Bergametti F, Denier C, Labauge P, et al. Mutations within the programmed cell death 10 gene cause cerebral cavernous malformations. Am J Hum Genet. 2005;76:42–51. [PubMed: 15543491]

10. Akers AL, Johnson E, Steinberg GK, Zabramski JM and Marchuk DA. Biallelic somatic and germline mutations in cerebral cavernous malformations (CCMs): evidence for a two-hit mechanism of CCM pathogenesis. Hum Mol Genet. 2009;18:919–30. [PubMed: 19088123]
11. Pagenstecher A, Stahl S, Sure U and Felbor U. A two-hit mechanism causes cerebral cavernous malformations: complete inactivation of CCM1, CCM2 or CCM3 in affected endothelial cells. Hum Mol Genet. 2009;18:911–8. [PubMed: 19088124]
12. Ren AA, Snellings DA, Su YS, et al. PIK3CA and CCM mutations fuel cavernomas through a cancer-like mechanism. Nature. 2021;594:271–276. [PubMed: 33910229]
13. Louvi A, Chen L, Two AM, Zhang H, Min W and Gunel M. Loss of cerebral cavernous malformation 3 (Ccm3) in neuroglia leads to CCM and vascular pathology. Proc Natl Acad Sci U S A. 2011;108:3737–42. [PubMed: 21321212]
14. Wang K, Zhang H, He Y, Jiang Q, Tanaka Y, Park IH, Pober JS, Min W and Zhou HJ. Mural Cell-Specific Deletion of Cerebral Cavernous Malformation 3 in the Brain Induces Cerebral Cavernous Malformations. Arterioscler Thromb Vasc Biol. 2020;40:2171–2186. [PubMed: 32640906]
15. Lopez-Ramirez MA, Lai CC, Soliman SI, et al. Astrocytes propel neurovascular dysfunction during cerebral cavernous malformation lesion formation. J Clin Invest. 2021.
16. McDonald DA, Shenkar R, Shi C, Stockton RA, Akers AL, Kucherlapati MH, Kucherlapati R, Brainer J, Ginsberg MH, Awad IA and Marchuk DA. A novel mouse model of cerebral cavernous malformations based on the two-hit mutation hypothesis recapitulates the human disease. Hum Mol Genet. 2011;20:211–22. [PubMed: 20940147]
17. Chan AC, Drakos SG, Ruiz OE, et al. Mutations in 2 distinct genetic pathways result in cerebral cavernous malformations in mice. J Clin Invest. 2011;121:1871–81. [PubMed: 21490399]
18. Cunningham K, Uchida Y, O'Donnell E, Claudio E, Li W, Soneji K, Wang H, Mukouyama YS and Siebenlist U. Conditional deletion of Ccm2 causes hemorrhage in the adult brain: a mouse model of human cerebral cavernous malformations. Hum Mol Genet. 2011;20:3198–206. [PubMed: 21596842]
19. Boulday G, Blecon A, Petit N, Chareyre F, Garcia LA, Niwa-Kawakita M, Giovannini M and Tournier-Lasserve E. Tissue-specific conditional CCM2 knockout mice establish the essential role of endothelial CCM2 in angiogenesis: implications for human cerebral cavernous malformations. Dis Model Mech. 2009;2:168–77. [PubMed: 19259391]
20. Maddaluno L, Rudini N, Cuttano R, et al. EndMT contributes to the onset and progression of cerebral cavernous malformations. Nature. 2013;498:492–6. [PubMed: 23748444]
21. Zhou Z, Tang AT, Wong WY, et al. Cerebral cavernous malformations arise from endothelial gain of MEKK3-KLF2/4 signalling. Nature. 2016;532:122–6. [PubMed: 27027284]
22. Voss K, Stahl S, Schleider E, Ullrich S, Nickel J, Mueller TD and Felbor U. CCM3 interacts with CCM2 indicating common pathogenesis for cerebral cavernous malformations. Neurogenetics. 2007;8:249–56. [PubMed: 17657516]
23. Draheim KM, Li X, Zhang R, Fisher OS, Villari G, Boggon TJ and Calderwood DA. CCM2-CCM3 interaction stabilizes their protein expression and permits endothelial network formation. J Cell Biol. 2015;208:987–1001. [PubMed: 25825518]
24. Wang K, Chen H, Zhou Z, Zhang H, Zhou HJ and Min W. ATPIF1 maintains normal mitochondrial structure which is impaired by CCM3 deficiency in endothelial cells. Cell Biosci. 2021;11:11. [PubMed: 33422124]
25. Denier C, Labauge P, Bergametti F, Marchelli F, Riant F, Arnoult M, Maciazek J, Vicaut E, Brunereau L and Tournier-Lasserve E. Genotype-phenotype correlations in cerebral cavernous malformations patients. Ann Neurol. 2006;60:550–6. [PubMed: 17041941]
26. Shenkar R, Shi C, Rebeiz T, et al. Exceptional aggressiveness of cerebral cavernous malformation disease associated with PDCD10 mutations. Genetics in medicine : official journal of the American College of Medical Genetics. 2014.
27. Zhou HJ, Qin L, Zhang H,Tet al. . Augmented endothelial exocytosis of angiopoietin-2 resulting from CCM3-deficiency contributes to the progression of cerebral cavernous malformation. Nat Med. 2016;22:1033–42. [PubMed: 27548575]
28. Tang AT, Sullivan KR, Hong CC, et al. Distinct cellular roles for PDCD10 define a gut-brain axis in cerebral cavernous malformation. Sci Transl Med. 2019;11:eaaw3521. [PubMed: 31776290]

29. Zhang Y, Tang W, Zhang H, Niu X, Xu Y, Zhang J, Gao K, Pan W, Boggon TJ, Toomre D, Min W and Wu D. A network of interactions enables CCM3 and STK24 to coordinate UNC13D-driven vesicle exocytosis in neutrophils. Developmental cell. 2013;27:215–26. [PubMed: 24176643]
30. Zhou HJ, Qin L, Jiang Q, Murray KN, Zhang H, Li B, Lin Q, Graham M, Liu X, Grutzendler J and Min W. Caveolae-mediated Tie2 signaling contributes to CCM pathogenesis in a brain endothelial cell-specific Pdcd10-deficient mouse model. Nat Commun. 2021;12:504. [PubMed: 33495460]
31. He Y, Zhang H, Yu L, Gunel M, Boggon TJ, Chen H and Min W. Stabilization of VEGFR2 signaling by cerebral cavernous malformation 3 is critical for vascular development. Sci Signal. 2010;3:ra26. [PubMed: 20371769]
32. You C, Sandalcioglu IE, Dammann P, Felbor U, Sure U and Zhu Y. Loss of CCM3 impairs DLL4-Notch signalling: implication in endothelial angiogenesis and in inherited cerebral cavernous malformations. J Cell Mol Med. 2013;17:407–18. [PubMed: 23388056]
33. Petrova TV, Karpanen T, Norrmen C, Mellor R, Tamakoshi T, Finegold D, Ferrell R, Kerjaschki D, Mortimer P, Yla-Herttuala S, Miura N and Alitalo K. Defective valves and abnormal mural cell recruitment underlie lymphatic vascular failure in lymphedema distichiasis. Nat Med. 2004;10:974–81. [PubMed: 15322537]
34. Sabine A, Agalarov Y, Maby-El Hajjami H, et al. Mechanotransduction, PROX1, and FOXC2 cooperate to control connexin37 and calcineurin during lymphatic-valve formation. Developmental cell. 2012;22:430–45. [PubMed: 22306086]
35. Zawieja DC. Contractile physiology of lymphatics. Lymphat Res Biol. 2009;7:87–96. [PubMed: 19534632]
36. Dumont DJ, Jussila L, Taipale J, Lymboussaki A, Mustonen T, Pajusola K, Breitman M and Alitalo K. Cardiovascular failure in mouse embryos deficient in VEGF receptor-3. Science. 1998;282:946–9. [PubMed: 9794766]
37. Karkkainen MJ, Haiko P, Sainio K, Partanen J, Taipale J, Petrova TV, Jeltsch M, Jackson DG, Talikka M, Rauvala H, Betsholtz C and Alitalo K. Vascular endothelial growth factor C is required for sprouting of the first lymphatic vessels from embryonic veins. Nat Immunol. 2004;5:74–80. [PubMed: 14634646]
38. Irrthum A, Karkkainen MJ, Devriendt K, Alitalo K and Vikkula M. Congenital hereditary lymphedema caused by a mutation that inactivates VEGFR3 tyrosine kinase. Am J Hum Genet. 2000;67:295–301. [PubMed: 10856194]
39. Evans AL, Bell R, Brice G, Comeglio P, Lipede C, Jeffery S, Mortimer P, Sarfarazi M and Child AH. Identification of eight novel VEGFR-3 mutations in families with primary congenital lymphoedema. J Med Genet. 2003;40:697–703. [PubMed: 12960217]
40. Norrmen C, Ivanov KI, Cheng J, Zangger N, Delorenzi M, Jaquet M, Miura N, Puolakkainen P, Horsley V, Hu J, Augustin HG, Yla-Herttuala S, Alitalo K and Petrova TV. FOXC2 controls formation and maturation of lymphatic collecting vessels through cooperation with NFATc1. J Cell Biol. 2009;185:439–57. [PubMed: 19398761]
41. Liu X, Pasula S, Song H, Tessneer KL, et al. , Srinivasan RS and Chen H. Temporal and spatial regulation of epsin abundance and VEGFR3 signaling are required for lymphatic valve formation and function. Sci Signal. 2014;7:ra97. [PubMed: 25314967]
42. Zhang Y, Ulvmar MH, Stanczuk L, Martinez-Corral I, Frye M, Alitalo K and Makinen T. Heterogeneity in VEGFR3 levels drives lymphatic vessel hyperplasia through cell-autonomous and non-cell-autonomous mechanisms. Nat Commun. 2018;9:1296. [PubMed: 29615616]
43. Flister MJ, Volk LD and Ran S. Characterization of Prox1 and VEGFR-3 expression and lymphatic phenotype in normal organs of mice lacking p50 subunit of NF-kappaB. Microcirculation. 2011;18:85–101. [PubMed: 21166921]
44. Chen L, Mupo A, Huynh T, Cioffi S, Woods M, Jin C, McKeehan W, Thompson-Snipes L, Baldini A and Illingworth E. Tbx1 regulates Vegfr3 and is required for lymphatic vessel development. J Cell Biol. 2010;189:417–24. [PubMed: 20439995]
45. Lee S, Kang J, Yoo J, Ganesan SK, Cook SC, Aguilar B, Ramu S, Lee J and Hong YK. Prox1 physically and functionally interacts with COUP-TFII to specify lymphatic endothelial cell fate. Blood. 2009;113:1856–9. [PubMed: 18815287]

46. Benedito R, Rocha SF, Woeste M, Zamykal M, Radtke F, Casanovas O, Duarte A, Pytowski B and Adams RH. Notch-dependent VEGFR3 upregulation allows angiogenesis without VEGF-VEGFR2 signalling. Nature. 2012;484:110–4. [PubMed: 22426001]
47. Jones D, Li Y, He Y, Xu Z, Chen H and Min W. Mirtron microRNA-1236 inhibits VEGFR-3 signaling during inflammatory lymphangiogenesis. Arterioscler Thromb Vasc Biol. 2012;32:633–42. [PubMed: 22223733]
48. Nilsson I, Bahram F, Li X, Gualandi L, Koch S, Jarvius M, Soderberg O, Anisimov A, Kholova I, Pytowski B, Baldwin M, Yla-Herttuala S, Alitalo K, Kreuger J and Claesson-Welsh L. VEGF receptor 2/−3 heterodimers detected in situ by proximity ligation on angiogenic sprouts. EMBO J. 2010;29:1377–88. [PubMed: 20224550]
49. Wang Y, Nakayama M, Pitulescu ME, Schmidt TS, Bochenek ML, Sakakibara A, Adams S, Davy A, Deutsch U, Luthi U, Barberis A, Benjamin LE, Makinen T, Nobes CD and Adams RH. Ephrin-B2 controls VEGF-induced angiogenesis and lymphangiogenesis. Nature. 2010;465:483–6. [PubMed: 20445537]
50. Zhou HJ, Chen X, Huang Q, Liu R, Zhang H, Wang Y, Jin Y, Liang X, Lu L, Xu Z and Min W. AIP1 mediates vascular endothelial cell growth factor receptor-3-dependent angiogenic and lymphangiogenic responses. Arterioscler Thromb Vasc Biol. 2014;34:603–15. [PubMed: 24407031]
51. Bazigou E, Lyons OT, Smith A, Venn GE, Cope C, Brown NA and Makinen T. Genes regulating lymphangiogenesis control venous valve formation and maintenance in mice. J Clin Invest. 2011;121:2984–92. [PubMed: 21765212]
52. Pitulescu ME, Schmidt I, Benedito R and Adams RH. Inducible gene targeting in the neonatal vasculature and analysis of retinal angiogenesis in mice. Nat Protoc. 2010;5:1518–34. [PubMed: 20725067]
53. Jones D, Xu Z, Zhang H, He Y, Kluger MS, Chen H and Min W. Functional analyses of the bone marrow kinase in the X chromosome in vascular endothelial growth factor-induced lymphangiogenesis. Arterioscler Thromb Vasc Biol. 2010;30:2553–61. [PubMed: 20864667]
54. Sabine A, Bovay E, Demir CS, et al. FOXC2 and fluid shear stress stabilize postnatal lymphatic vasculature. J Clin Invest. 2015;125:3861–77. [PubMed: 26389677]
55. Harvey NL. The link between lymphatic function and adipose biology. Ann N Y Acad Sci. 2008;1131:82–8. [PubMed: 18519961]
56. Oliver G, Kipnis J, Randolph GJ and Harvey NL. The Lymphatic Vasculature in the 21(st) Century: Novel Functional Roles in Homeostasis and Disease. Cell. 2020;182:270–296. [PubMed: 32707093]
57. Detter MA, Snellings DA and Marchuk DA. Cerebral Cavernous Malformations Develop Through Clonal Expansion of Mutant Endothelial Cells. Cir Res. 2018;123:1143–51.
58. Malinverno M, Maderna C, Abu Taha A, Corada M, Orsenigo F, Valentino M, Pisati F, Fusco C, Graziano P, Giannotta M, Yu QC, Zeng YA, Lampugnani MG, Magnusson PU and Dejana E. Endothelial cell clonal expansion in the development of cerebral cavernous malformations. Nat Commun. 2019;10:2761. [PubMed: 31235698]
59. Fournier E, Blaikie P, Rosnet O, Margolis B, Birnbaum D and Borg JP. Role of tyrosine residues and protein interaction domains of SHC adaptor in VEGF receptor 3 signaling. Oncogene. 1999;18:507–14. [PubMed: 9927207]
60. Salameh A, Galvagni F, Bardelli M, Bussolino F and Oliviero S. Direct recruitment of CRK and GRB2 to VEGFR-3 induces proliferation, migration, and survival of endothelial cells through the activation of ERK, AKT, and JNK pathways. Blood. 2005;106:3423–31. [PubMed: 16076871]
61. Dixelius J, Makinen T, Wirzenius M, Karkkainen MJ, Wernstedt C, Alitalo K and Claesson-Welsh L. Ligand-induced vascular endothelial growth factor receptor-3 (VEGFR-3) heterodimerization with VEGFR-2 in primary lymphatic endothelial cells regulates tyrosine phosphorylation sites. J Biol Chem. 2003;278:40973–9. [PubMed: 12881528]
62. Deng Y, Zhang X and Simons M. Molecular controls of lymphatic VEGFR3 signaling. Arterioscler Thromb Vasc Biol. 2015;35:421–9. [PubMed: 25524775]
63. Hayden MS and Ghosh S. Shared principles in NF-kappaB signaling. Cell. 2008;132:344–62. [PubMed: 18267068]

64. Liang P, Zhang H, Wang G, Li S, Cong S, Luo Y and Zhang B. KPNB1, XPO7 and IPO8 mediate the translocation ofNF-kappaB/p65 into the nucleus. Traffic. 2013;14:1132–43. [PubMed: 23906023]

65. Moroianu J Nuclear import and export pathways. J Cell Biochem. 1999;Suppl 32–33:76–83.

66. Tang AT, Choi JP, Kotzin JJ, et al. Endothelial TLR4 and the microbiome drive cerebral cavernous malformations. Nature. 2017;545:305–310. [PubMed: 28489816]

67. Olsson AK, Dimberg A, Kreuger J and Claesson-Welsh L. VEGF receptor signalling - in control of vascular function. Nat Rev Mol Cell Biol. 2006;7:359–71. [PubMed: 16633338]

68. Lapinski PE, Kwon S, Lubeck BA, Wilkinson JE, Srinivasan RS, Sevick-Muraca E and King PD. RASA1 maintains the lymphatic vasculature in a quiescent functional state in mice. J Clin Invest. 2012;122:733–47. [PubMed: 22232212]

HIGHLIGHTS

- CCM3 loss of lymphatic endothelial cells induces lymphatic hyperplasia and malformation in mouse models.
- CCM3 deletion augments NF-κB nuclear translocation and NF-κB-mediated VEGFR3 expression in lymphatic endothelial cells.
- Inhibition of VEGFR3 rescues the lymphatic defects in structure and function in the CCM3-deficient mouse models, uncovering a novel function of CCM3 in lymphatics.

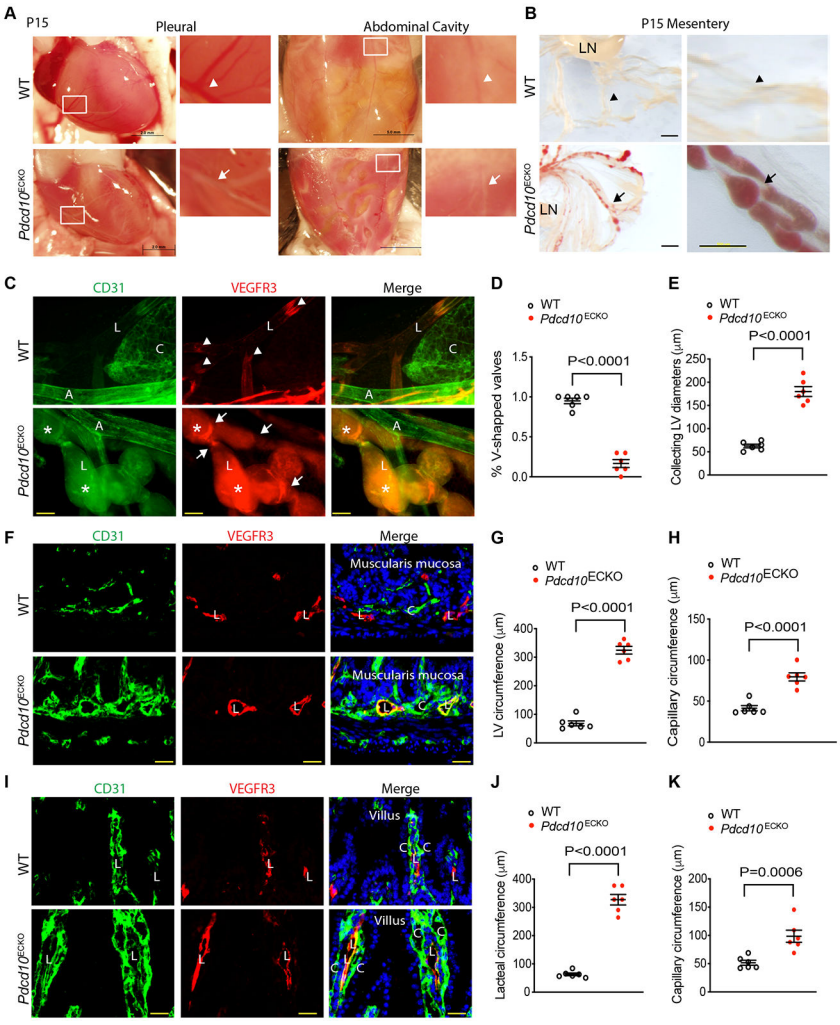

Fig. 1. Inducible EC-specific *Pdcd10* deletion (*Pdcd10*^{ECKO}) causes defects in both blood and lymphatic vessels in various organs.

A. Gross images of abdominal cavity and heart of *Pdcd10*$^{fl/fl}$ (WT) and *Pdcd10*^{ECKO} mice at P15. Chyle blood in the thoracic (pleural) and chyle ascites (milky peritoneal cavity) in *Pdcd10*^{ECKO} are indicated by arrows while normal heart and cavity by arrowheads in WT. Higher magnifications of images within the boxes are shown. Arrowheads and arrows point vessels with normal blood in WT and vessels with chyle blood vessel in *Pdcd10*^{ECKO} mice, respectively. **B**. Images of mesentery lymphatics with dilation and blood infusion in *Ccm3*^{ECKO} mice. Arrowheads indicate normal lymphatics while arrows indicate blood-filled lymphatics. **C**. Immunofluorescence staining with CD31 and VEGFR3 for mesentery lymphatics at P15. Arrowheads indicate V-shaped valves while arrows indicate abnormal valves. Asterisks indicate dilated lymphatics. **D**. Quantification of percentages of V-shaped valve numbers in P15 mesentery. 10 vessels per mouse were counted. **E**. Average diameters of collecting lymphatics in P15 mesentery. 10 vessels per mouse were counted. **F-K**. immunofluorescence staining for microvessels and lymphatics by CD31 and VEGFR3 in the intestine wall (F) and villi (I) at P15. Quantifications of capillary and lymphatic circumferences in intestine walls (G-H) and villi (J-K). A: artery; V: vein; C: capillary; L:

lymphatics/lacteals; LN: lymph node. All values are mean ± SEM. n=6 mice per group; 3 sections from each mouse and 5 fields per section were quantified. *P* values are indicated, using by unpaired, two tailed Student's t-test. Scale bar: 2 mm (A, pleural); 3 mm (A, abdominal cavity); 500 μm (B); 100 μm (C); 50 μm (F, I).

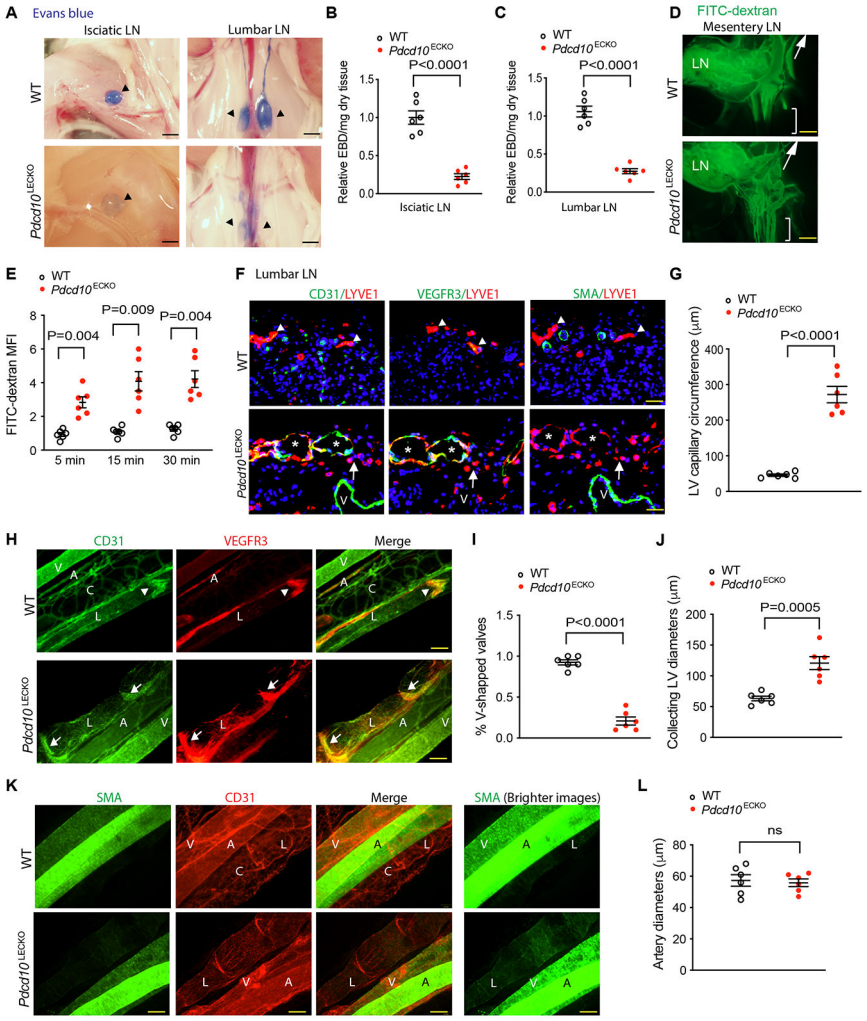

Fig. 2. Inducible *Pdcd10* deletion in lymphatic EC (*Pdcd10*^{LECKO}) induces lymphatic dysfunction without blood vascular leakage.

A-C. Lymphatic transport function. A. Representative images of isciatic and lumbar lymph nodes (arrows) after Evans blue injection into hind foot pads of P30 wild-type and *Pdcd10*^{LECKO} mice. B-C. Quantification of Evans blue dye (relative EBD/mg dry tissue) in the isciatic and lumbar LNs (n=6 mice per group). **D-E.** Backflow assay. D. Representative images of mesentery lymphatic drainage after FITC-Dextran injection in P30 WT and *Pdcd10*^{LECKO} mice. Arrows indicate the FITC-dextran transported up to thoracic ducts. Brackets indicate a backflow in *Pdcd10*^{LECKO} but was not detected in WT mice. **E**. Quantification of FITC-Dextran (mean fluorescence intensity) at various times after injection, by taking WT 5 min as 1.0 (n=6 mice per group). **F-G**. Lumbar lymphatics. F. A serial sections were immunostained with various markers as indicated. Arrowheads indicate normal lymphatics while asterisks indicate dilated lymphatics. Arrows indicate individual LYVE1^{+} lymphatic ECs or macrophages. n=6 mice per group; LV capillary circumferences were quantified from 3 sections of each mouse and 5 fields per section. **H-J**. P15 mesentery whole mount staining with CD31 and VEGFR3. H. Arrowheads indicate V-shaped valves while arrows indicate abnormal valves. I. Quantification of percentages of V-shaped valve

numbers in P15 mesentery. J. Average diameters of collecting lymphatics. n=6 mice per group. **K-L**. P15 mesentery whole mount staining with CD31/SMA. Brighter images of SMA are presented at the right panels (K). L. Quantifications of artery diameters. 10 vessels per mouse were counted. A: artery; V: vein; C: capillary; L: lymphatics/lacteals; LN: lymph node. Data are means ± SEM. P values are indicated, using unpaired, two-tailed Student's t-test except 2E with two-way ANOVA followed by Sidak's multiple comparisons test. ns: non-significant. Scale bar: 2 mm (A); 500 μm (D); 100 μm (H, K). 50 μm (F).

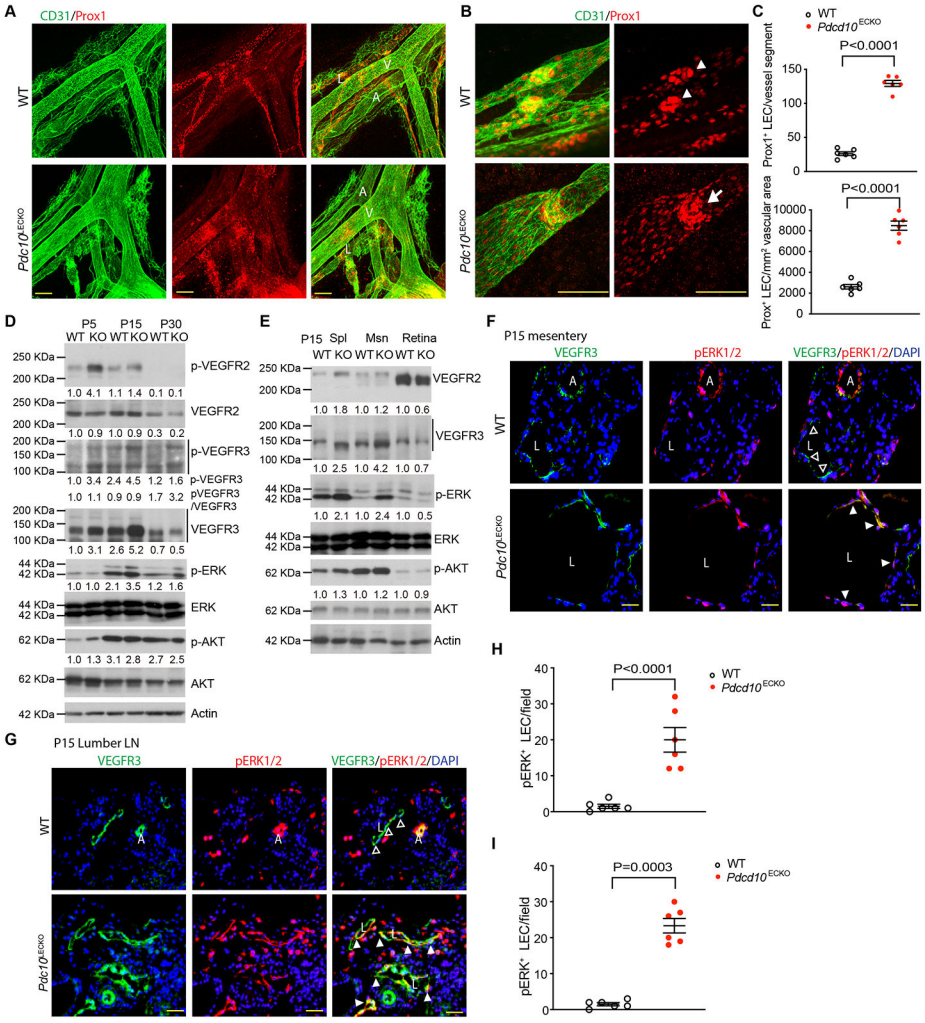

Fig. 3: *Pdcd10*$^{\text{LECKO}}$ exhibit lymphatic hyperplasia with increased VEGFR3-ERK1/2 signaling.

A-C. Lymphatic hyperplasia. A. P30 mesentery tissues were subjected to whole mount staining with CD31 and Prox1. B. High power images are shown. Arrowheads indicate V-shaped valves while arrows indicate abnormal valves. C. Prox1^{+} LEC/lymphatic vessel and Prox1^{+} cells/mm^{2} lymphatic vessel area were quantified. n=6 mice per group. 10 vessels per mouse were counted. **D**. Time course of VEGFR3-ERK1/2 in mesentery. P5, P15 and P30 mesentery tissue lysates were subjected to Western blot with respective antibodies. Protein levels and phospho- /total protein ratios were quantified and presented as fold changes by taking WT P5 as 1.0. n=3 mice per group. **E**. VEGFR3 signaling in tissues. Tissues lysates of P15 spleen, mesentery and retina were subjected to Western blot with respective antibodies. Protein levels and phospho- /total protein ratios were quantified and presented as fold changes by taking WT P5 as 1.0. n=3 mice per group. **F-I**. VEGFR3-ERK1/2 activation in mesentery lymphatics (F) and lumbar LN (G) by immunostaining. Solid arrowheads indicate VEGFR3^{+}pERK^{+} LECs *Pdcd10*$^{\text{LECKO}}$ mice while open arrowheads for VEGFR3^{+}pERK^{-} LEC in WT. H-I. Quantifications of VEGFR3^{+}pERK^{+} LECs/field. n=6 mice per group; 3 sections from each mouse and 5 fields per section were quantified. A:

artery; V: vein; L: lymphatics/lacteals. Data are means ± SEM. *P* values are indicated, using unpaired, two-tailed Student's t-test. Scale bar: 100 μm (A, B); 50 μm (F, G).

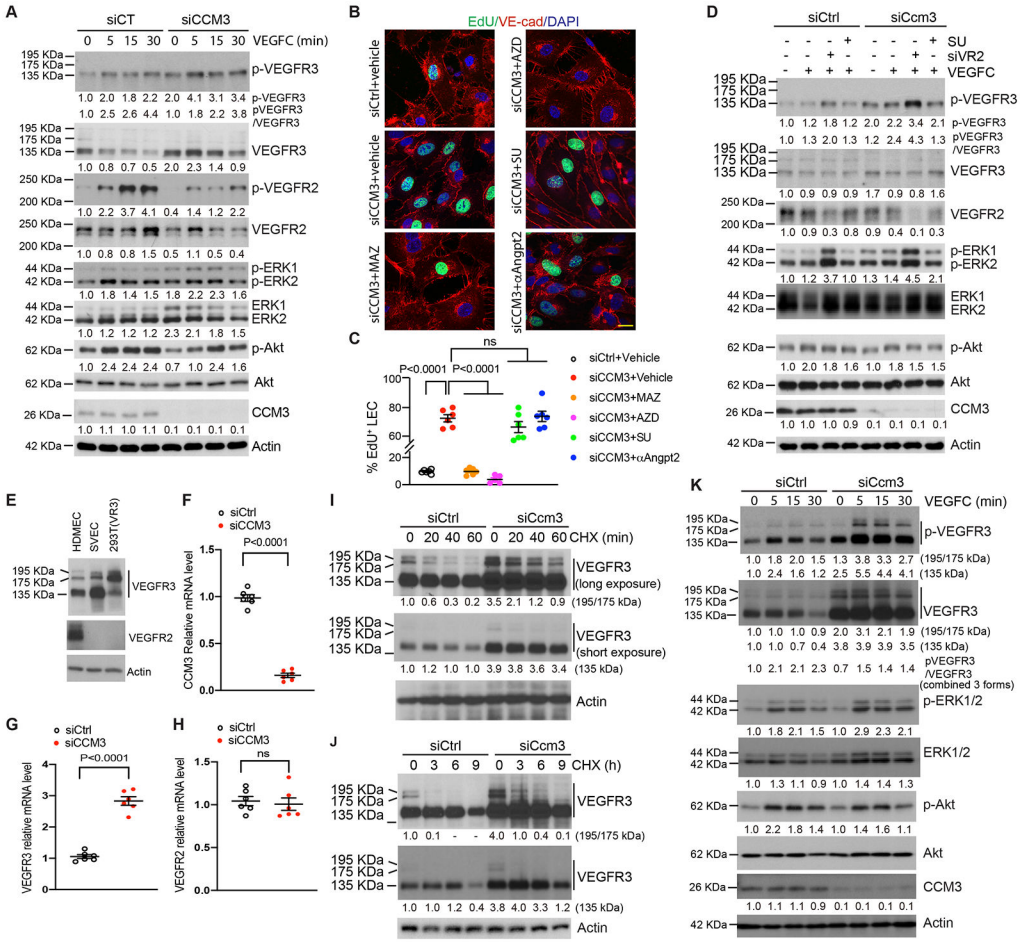

Fig. 4. Regulation of VEGFR3 signaling regulation in lymphatic ECs.

A. Increased VEGFR3-ERK1/2 signaling by CCM3 silencing in HDMEC. HDMECs were transfected with siCtrl or siCCM3 for 36 h followed by serum starvation for 12 h. The cells were treated with VEGF-C (50 ng/ml) for indicated times and cell lysates were subjected to Western blotting for the VEGFRs signaling. Protein levels and phospho- /total protein ratios were quantified and presented as fold changes by taking siCtrl 0 min as 1.0. n=3 from three independent experiments. **B-C**. Role of VEGFR3-ERK1/2 in LEC proliferation in vitro. HDMEC were transfected with control or CCM3 siRNAs for 36 h. Cells were treated by various inhibitors (VEGFR3 inhibitor MAZ51, VEGFR2 inhibitor SU5402, ERK1/2 upstream MEK1 inhibitor AZD6244 or Angiopoietin-2 neutralization antibody) as indicated for 12 h and LEC proliferation was determined by an EdU incorporation assay. Representative images are presented in (B) and % EdU^+ LEC are quantified in (C). n=6 replicates from two independent experiments. Scale bar: 50 μm (B). **D**. Effects of VEGFR2 depletion on VEGFR3-ERK1/2 activation in LECs. HDMEC were transfected with control or CCM3 siRNAs in the presence of Vegfr2 siRNA or VEGFR2 kinase inhibitor SU5402. The cells were treated with VEGF-C for 5 min and cell lysates were subjected to Western blotting for the VEGFRs signaling. Protein levels and phospho- /total protein ratios were quantified and presented as fold changes by taking untreated siCtrl as 1.0. n=3. **E.** Expressions of VEGFR3 in mouse LEC line SVEC4-10. Cell lysates were subjected

to Western blot for VEGFRs expression. 293T lysate with VEGFR3 overexpression from a plasmid was used as a control. Three bands of VEGFR3 (195, 175 and 135 kDa) were indicated. **F-H**. Effects of CCM3 silencing on VEGFR3 mRNA in SVEC4-10. SVEC4-10 were transfected with siCtrl or siCCM3. CCM3, VEGFR2 and VEGFR3 mRNAs were determined by qRT-PCR. Relative mRNA was presented by taking siCtrl as 1.0. n=6. **I-J**. Half-life of VEGFR3 protein in SVEC4-10. SVEC4-10s were incubated in the presence of cycloheximide for indicated times and VEGFR3 protein was determined. Protein levels and phospho- /total protein ratios were quantified and presented as fold changes by taking siCtrl 0 min as 1.0. n=3 from three independent experiments. **K**. Increased VEGFR3-ERK1/2 signaling by siCCM3 in SVEC cells. SVEC4-10 were transfected with siCtrl or siCCM3 for 36 h. Cells were serum-starved for 12 h followed by VEGF-C treatment for indicated times. VEGFRs signaling was determined, and protein levels and phospho- /total protein ratios were quantified and presented as fold changes by taking untreated siCtrl as 1.0. n=3 from three independent experiments. *P* values are indicated, using one-way ANOVA followed by Bonferroni's post-hoc test (C) or unpaired, two-tailed Student's t-test (F, G, H). ns: non-significant.

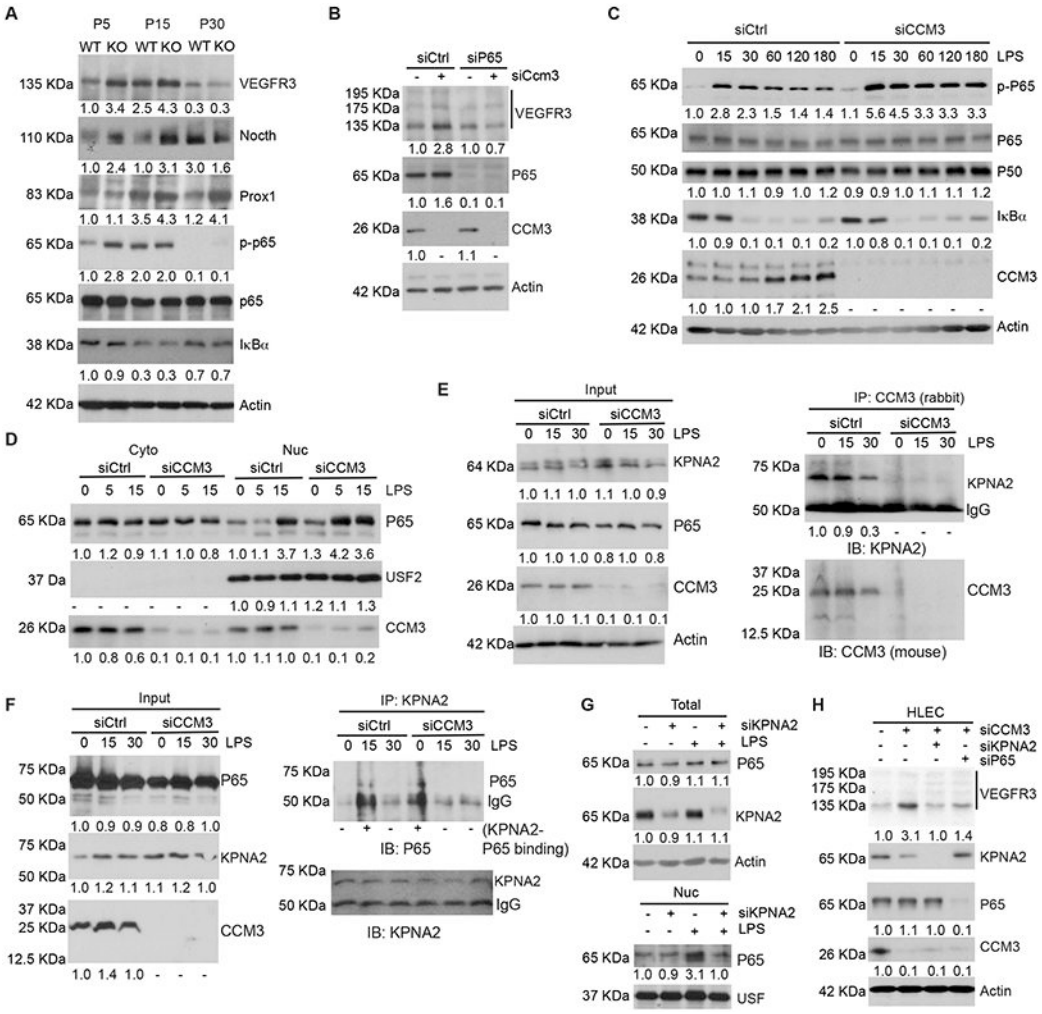

Fig. 5. CCM3 regulates NF-κB nuclear translocation and NF-κB-dependent VEGFR3 transcription in LEC.

A. Expression and activation of transcriptional factors involved in VEGFR3 expression. Mesentery lysates were subjected to Western blotting with respective antibodies. Protein levels and phospho- /total protein ratios were quantified and quantified as fold changes by taking WT P5 as 1.0. n=3 mice per group. **B**. Role of P65 in VEGFR3 expression. HDMECs were transfected with siCtrl or siCCM3 in the absence or presence of P65 siRNAs, and VEGFR3 protein was determined by Western blotting. Relative protein levels and phospho- /total protein ratios were quantified by taking WT as 1.0. n=3 from three independent experiments. **C**. CCM3 in NFκB signaling. siCtrl and siCCM3-transfected HDMECs were treated with LPS (10 ng/ml) for indicated times. NFκB signaling was determined with respective antibodies. Relative protein levels and phospho- /total protein ratios were quantified by taking untreated siCtrl as 1.0. n=3 from three independent experiments. **D**. P65 nuclear translocation. siCtrl and siCCM3-transfected HDMECs were treated with LPS for indicated times. Cytosolic and nuclear fractions were prepared and P65 protein was determined. A nuclear protein USF2 and cytosolic CCM3 were used as controls. (−): undetectable. Relative protein levels were quantified by taking untreated

siCtrl as 1.0. n=3 from three independent experiments. **E**. CCM3-KPNA2 interactions. siCtrl and siCCM3 HDMECs lysates (input) were subjected to co-immunoprecipitation with anti-CCM3 (rabbit) followed by Western blot with anit-KPNA2 or anti-CCM3 (mouse). Relative protein levels were quantified by taking untreated siCtrl as 1.0. n=3 from three independent experiments. (−): undetectable. **F**. CCM3 regulates KPNA2-P65 interactions. siCtrl and siCCM3-transfected HDMECs were treated with LPS for indicated times. HDMECs lysates (input) were subjected to co-immunoprecipitation with anti-KPNA2 followed by Western blot with anit-P65. (+) and (−) indicate positive and negative in the KPNA2-P65 binding, respectively. n=3 from three independent experiments. **G**. KPNA2 in P65 nuclear translocation. siCtrl (−) and siKPNA2-transfected HDMECs were untreated or treated with LPS (10 ng/ml for 30 min). Total and nuclear lysates were subjected to Western blot. Relative P65 protein levels were quantified by taking siCtrl as 1.0. n=3 from three independent experiments. **H.** Role of KPNA2 in VEGFR3 expression. HDMECs were transfected with siCtrl (−) or siCCM3 in the presence of siKPNA2 or siP65. Protein levels were determined by Western blot with respective antibodies and quantified by taking siCtrl as 1.0. n=3 from three independent experiments.

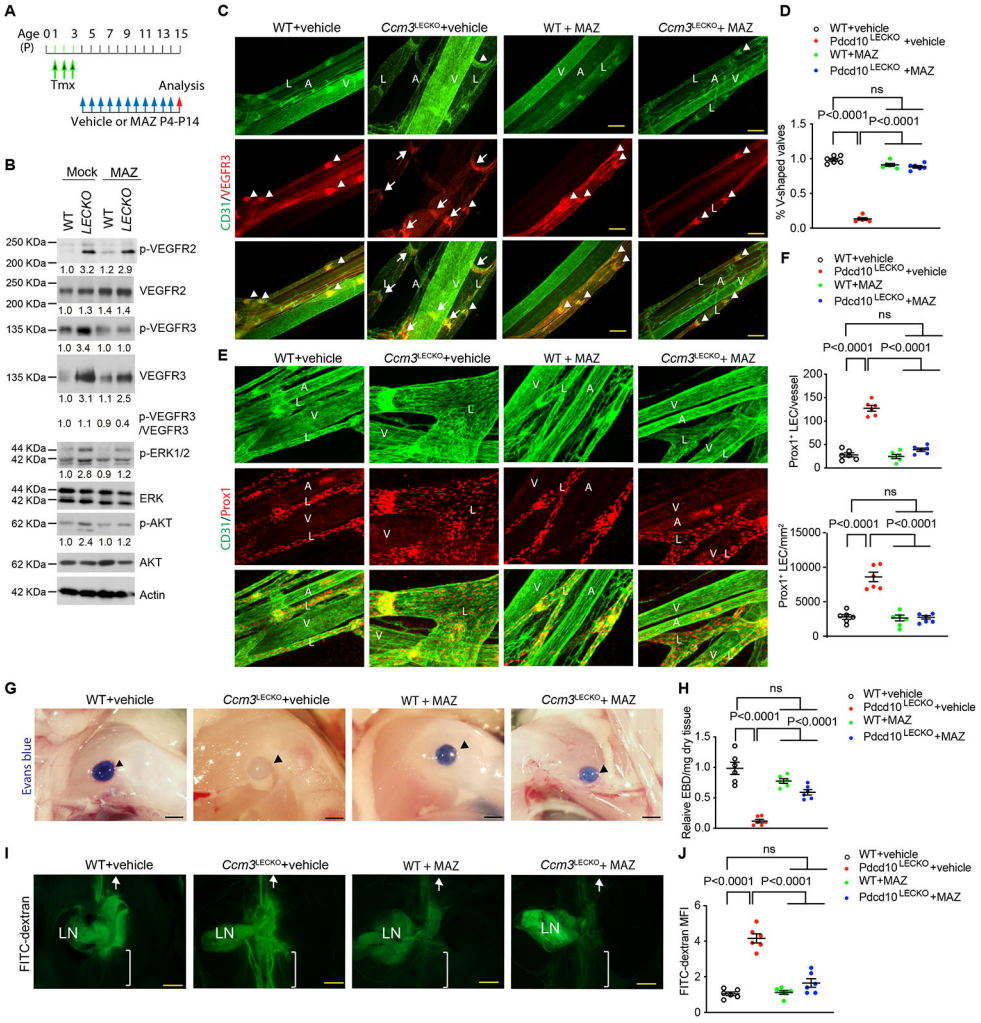

Fig. 6. Inhibition of VEGFR3-ERK1/2 signaling rescues the lymphatic hyperplasia in *Pdcd10*^{LECKO} mice.

A. A diagram for the VEGFR3 inhibitor protocol. WT and *Pdcd10*^{LECKO} mice were received intraperitoneal injection of vehicle or VEGFR3 inhibitor MAZ51 compound at 5 μg/g body weight daily from P2-P14. Mice were subjected to analyses at P15-P30. **B**. P15 mesentery tissue lysates were subjected to Western blotting with respective antibodies. Protein levels and phospho- /total protein ratios were quantified and presented as fold changes by taking WT vehicle as 1.0. n=3 mice per group. **C.** Mesentery tissues were subjected to whole mount staining with CD31 and VEGFR3. Arrowheads indicate V-shaped valves while arrows indicate abnormal valves. **D**. Quantifications of % V-shaped valves. n=6 mice per group. 10 vessels per mouse were counted. **E.** Mesentery tissues were subjected to whole mount staining with CD31 with Prox1. **F**. Prox1^{+} LEC/lymphatic vessel and Prox1^{+} cells/lymphatic vessel area (mm^{2}) were quantified. n=6 mice per group. **G-J**. Lymphatic function assays in P30 mice. **G-H**. Lymphatic transport function. G. Representative images of isciatic lymph nodes (arrows) after Evans blue injection into hind foot pads of P30 wild-type and *Pdcd10*^{LECKO} mice. H. Quantification of Evans blue dye (relative EBD/mg dry tissue) in the isciatic LNs (n=6 mice per group). **I-J.** Backflow assay.

I. Representative images of mesentery lymphatic drainage after FITC-Dextran injection in P30 WT and *Pdcd10*^{LECKO} mice. Arrows indicate the FITC-dextran transported up to thoracic ducts. Brackets indicate a backflow in *Pdcd10*^{LECKO} but was not detected in WT mice. **J**. Quantification of FITC-Dextran (mean fluorescence intensity) at various times after injection, by taking WT 5 min as 1.0 (n=6 mice per group). A: artery; V: vein; L: lymphatics/lacteals. Data are means ± SEM. *P* values are indicated, using one-way ANOVA followed by Bonferroni's post-hoc test (D, F, H, J). Scale bar: 100 μm (C, E); 2 mm (G); 500 μm (I).

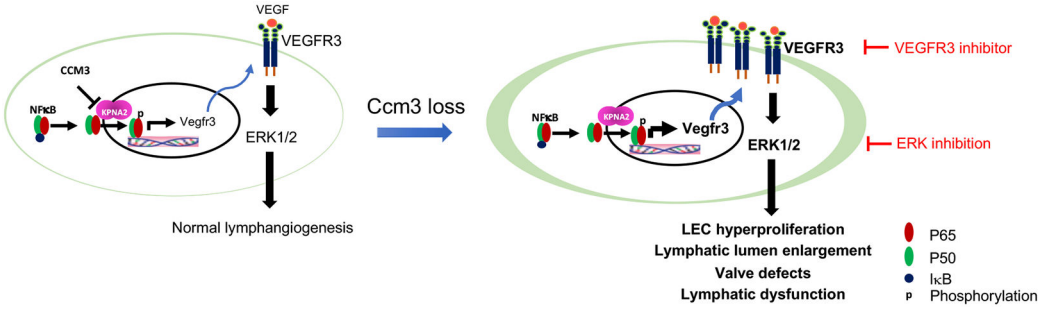

Fig.7: A model for CCM3 regulated VEGFR3 expression and lymphatic function.

CCM3 in lymphatic ECs (LECs) binds to KPNA2, limiting NF-κB nuclear translocation. CCM3 loss in LECs releases KPNA2 and causes nuclear accumulation of NF-κB and VEGFR3 expression. Augmented VEGFR3-ERK signaling induces LEC hyper-proliferation, valve malformation and lymphatic dysfunction. Blockade of VEGFR3 or ERK ameliorates lymphatic defects in the mouse models.